Revisiting GeV-scale annihilating dark matter with the AMS-02 positron fraction

Iason Krommydas[1,2,*] and Ilias Cholis[3,†]

[1]*Physics Division, National Technical University of Athens, Zografou, Athens 15780, Greece*
[2]*Department of Physics and Astronomy, Rice University, Houston, Texas 77005, USA*
[3]*Department of Physics, Oakland University, Rochester, Michigan 48309, USA*

(Received 23 October 2022; accepted 14 December 2022; published 4 January 2023)

Antimatter cosmic rays are used to probe new phenomena in physics, including dark matter annihilation. We use the cosmic-ray positron fraction spectrum by the Alpha Magnetic Spectrometer, to search for such an annihilation signal in the Galaxy. We focus on dark matter with mass between 5 GeV and 120 GeV, producing high-energy electrons and positrons. In these cosmic-ray energies the interplay of multiple astrophysical sources and phenomena, makes this search highly sensitive to the underlying astrophysical background assumptions. We use a vast public library of astrophysical models for the cosmic-ray positron fraction background, to derive robust upper limits on the dark matter's annihilation cross section for a number of annihilation channels. This library accounts for different types of cosmic-ray sources and uncertainties on their distribution in space and time. Also, it accounts for uncertainties on those sources' output, their injected into the interstellar medium cosmic-ray spectra and for uncertainties on cosmic-ray propagation. For any given dark matter particle mass and annihilation channel, upper limits on the annihilation cross section are given by bands that stretch a full order of magnitude in its value. Our work provides weaker limits compared to earlier results, that are however robust to all the relevant astrophysical uncertainties. Between 5 GeV and 15 GeV, we find indications for a possible excess flux of cosmic-ray electrons and positrons. That excess is found for most, but not all of our astrophysical background parameter space, and its significance can vary appreciably. Further scrutiny is necessary to improve the understanding of these lower-energy cosmic rays. Finally, we note that even if an excess signal is found in these energies, the current background uncertainties do not allow us to accurately deduce its underlying particle properties.

DOI: 10.1103/PhysRevD.107.023003

I. INTRODUCTION

Dark matter has been observed in a variety of astrophysical systems through its gravitational impact, in scales from as small as dwarf galaxies to as large as colliding galaxy clusters [1–13]. In addition, through detailed measurements of the cosmic microwave background (CMB), we know that dark matter accounts for about 27% of the critical density in the Universe, corresponding to about 85% of its matter [14–18]. Furthermore, accurate measurements probing big bang nucleosynthesis, the evolution of structures in the universe, observations on the mass distribution of different gravitationally collapsed structures and observations of the Layman-alpha forest, set a strong preference for what is referred to as "cold dark matter" [11,14,16,19–29]. However, the nature of dark matter remains a puzzle, with its mass ranging from 10^{-22} eV to as large as $O(10)\ M_{\odot}$ [30–54].

One class of dark matter candidates includes weakly interacting massive particles (WIMPs), that were thermally produced in the early universe through approximately electroweak scale interactions with Standard Model particles and a mass very approximately of $O(10)$ GeV–$O(10)$ TeV [45,47,55–57]. In this paper, we focus on the lower end of that mass range, probing dark matter with mass from 5 GeV and up to 120 GeV. For such dark matter particles we constrain the annihilation cross section they may have to leptons and to bottom quarks. Bottom quarks would be the prominent annihilation product for dark matter in that mass range, if dark matter couples to the Higgs boson [58]. These dark matter masses are interesting to search for, also because excesses in gamma rays [59–70] and in cosmic-ray antiprotons [71–74] have been claimed to be compatible with WIMPs in that mass range. We use the most recent measurements of the cosmic-ray positron fraction, i.e., the ratio of the positron flux over the electron plus positron flux, versus those particle's energy; made by the Alpha Magnetic Spectrometer (AMS-02) on board the International Space Station [75,76].

*ik23@rice.edu
†cholis@oakland.edu

Over the last decades antimatter cosmic-ray measurements have been used to probe possible dark matter signals [77–81]. Such cosmic rays are produced from rare inelastic collisions between cosmic-ray nuclei with the interstellar medium (ISM) gas and are commonly referred to as secondary cosmic rays. Primary cosmic rays are instead accelerated in supernova remnant (SNR) environments. A hypothetical dark matter particle in the GeV–TeV mass scale annihilating (or decaying) and producing among other byproducts antimatter cosmic rays, may give a detectable additional flux in measurements of such particles. This is the focus of this work. Dark matter particles producing cosmic-ray positrons could cause a feature in the positron flux and positron fraction. The qualities of such a feature, depend on the dark matter particle's mass, annihilation cross section and channel, i.e., the fist generation of Standard Model particles produced from the annihilation event. Dark matter originated features may be as small as a localized in energy, to give a few % bump on the positron fraction, or as wide in energy and large in amplitude as the entire rising above 5 GeV positron fraction spectrum.

Inversely, using the AMS-02 positron fraction's relatively smooth spectrum, one can set upper limits on the annihilation cross section of dark matter particles. That is done for a range of masses and a variety of annihilation channels [82–85]. This is the main aim of this paper.

The origin of the rising above 5 GeV positron fraction spectrum that was first measured by the Payload for Antimatter Matter Exploration and Light-nuclei Astrophysics (PAMELA) satellite [86,87], then confirmed by the Fermi-LAT [88] and further measured with an unprecedented accuracy by AMS-02 [75,89,90], has been a subject of great interest. One explanation for the additional positron flux, is relatively close-by "young" and "middle-aged" Milky Way pulsars that during their pulsar wind nebula (PWN) phase converted an appreciable fraction $[O(0.01) - O(0.1)]$ of their rotational energy into high-energy cosmic-ray electrons (e^-) and positrons (e^+) [91–109]. Another explanation is Milky Way SNRs, that in their first $O(10)$ kyr produced and accelerated secondary cosmic rays including positrons [110–118] (see however [119–122]). Furthermore, detailed modifications on the distribution of cosmic-ray sources and the propagation of cosmic rays through the ISM [123–125] and annihilating or decaying dark matter models have been explored to explain the positron fraction measurement [102,126–145]. We assume in this work that the overall rise of the positron fraction, shown with its AMS-02 measurement in Fig. 1, is not caused by dark matter, but instead from a more conventional source; a population of Milky Way pulsars.

Pulsars are localized sources of cosmic-ray electrons and positrons. Due to their rapid spin-down, pulsars convert their initial rotational energy into cosmic-ray $e^{\pm}$ and subsequently release those $e^{\pm}$ into the ISM in a comparatively short amount of time.[1] That makes pulsars cosmic-ray $e^{\pm}$ sources approximately localized both in space and time. High-energy $e^{\pm}$ lose rapidly their energy through synchrotron radiation and inverse Compton scattering as they interact with the ISM and before reaching us. That results in an upper-energy cutoff, on the $e^{\pm}$ spectra from individual pulsars [96,97,99]. In turn, a population of pulsars that could collectively explain the rising positron fraction spectrum, could also give spectral features at the higher energies where the number of contributing pulsars is reduced to the point of individual sources dominating narrow parts of that spectrum [97,99,105,109]. Such features can then be searched for as in [147]. Similar arguments can be made for PWNe. However, their expected higher-energy cutoffs are less sharp by comparison [118]. We use modeled populations of Milky Way pulsars produced in our earlier work of [109]. In Ref. [109], a library of publicly available pulsar population models was created that is in agreement with the cosmic-ray $e^{\pm}$ flux spectral measurements from AMS-02 [75,76],

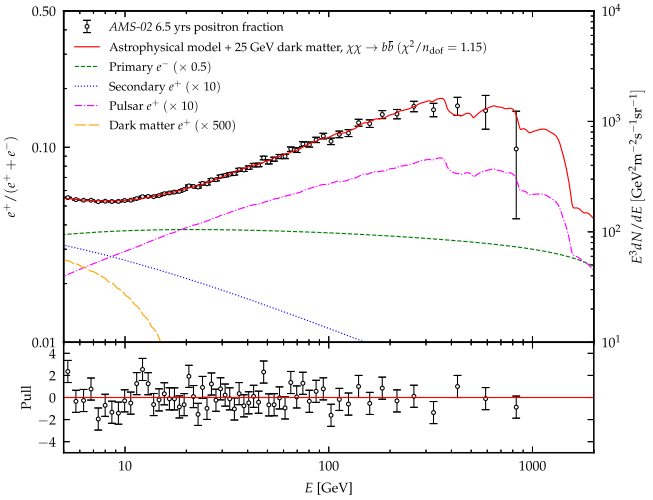

FIG. 1. The fit of a pulsar model from Ref. [109], to the *AMS-02* positron fraction after including the contribution from 25 GeV dark matter that annihilates to $b\bar{b}$. On the right y-axis in units of $E^3 dN/dE$ where dN/dE is the differential cosmic-ray flux, we show the solar modulated contribution from primary e^-, secondary e^+, pulsar e^+, and e^+ fluxes originating from dark matter annihilation scaled by some appropriate arbitrary factors from their best fit normalization to make them well visible. The secondary, pulsar and dark matter e^- fluxes are not shown since they are only slightly different due to solar modulation. We also show the pull $[(\text{data} - \text{model})/\sigma_{\text{data}}]$ distribution of the fit at the bottom.

[1]The time required for most cosmic-ray $e^{\pm}$ produced around the PWN environments to be released into the ISM, is at least an order of magnitude smaller than the propagation time required for these cosmic rays to reach our detectors [97]. The only exception would be a very close $[O(10)$ pc] pulsar (see however [146]).

the CALorimetric Electron Telescope (CALET) [148] and the DArk Matter Particle Explorer (DAMPE) telescope [149], as well as the AMS-02 positron fraction spectrum [90]. As the pulsar's contribution to the positron fraction spectrum is not perfectly smooth and with uncertainties, we use a library of models instead of just one generic parameterization. As we will show, we derive more conservative and more realistic limits on the dark matter annihilation cross section.

We note that in the models of Ref. [109], the production and propagation of the primary electron component coming from SNRs and the secondary electron and positron components coming from inelastic collisions of cosmic-ray nuclei with the ISM gas, were evaluated using GALPROP v54 [150,151]. In our fitting procedure to the AMS-02 data, we allowed for additional freedoms related to the injection power-laws of each of these components and each of their normalization (see Ref. [109] for further details). Instead, the electrons and positrons originating from the many thousands of individual randomly located and born local pulsars with their unique injection power and spectra was done separately following the prescription of [97,147]. The propagation codes used for the pulsars and the cosmic-ray primaries and secondaries are thus not identical. Their difference lies predominantly on the fact that GALPROP gives a sophisticated spatial profile for the distribution of the interstellar radiation field [152,153] (see also [154] for further updates) and the galactic magnetic field, while the pulsar propagation code takes a more simplified treatment using and averaged and uniform value for each. This uniform value is in agreement with the averaged GALPROP expectations for the local part of the Milky Way, but neglects any gradients in the energy density of the radiation field and the magnetic field at the benefit of providing us the ability to simulate the contribution of thousands of pulsars in unique locations, of unique ages and injection properties. To the level that we retain our discussion within a few kiloparsec (kpc) from the Sun, these gradients are of small impact to our derived limits.

In Sec. II, we discuss the general methodology of our approach, including the observations that we use, the astrophysical background modeling of the positron fraction and the statistical treatment followed in fitting the data. We also create mock positron fraction data to answer the question on the robustness of the positron fraction measurement as a means to study the particle properties of dark matter. Then in Sec. III, we present the results of searching for a possible dark matter signal in the positron fraction. We find that the limits on the annihilation cross section are not well defined. That is due to the underlying astrophysical background uncertainties. The annihilation cross section limits have a width that is at least one order of magnitude in the mass range of 5 GeV to 120 GeV that we study. In addition, we find indications for a possible excess of 5–15 GeV in cosmic-ray energy $e^{\pm}$. That excess while compatible with a WIMP-scale dark matter signal, has a significance that varies with the astrophysical background modeling and is not claimed to be a robust one. Further scrutiny will be required as cosmic-ray physics in that energy range improve with future observations. Moreover, in Sec. III, we perform our mock positron fraction analysis. We find that if dark matter contributes to the positron fraction spectrum at the few percent level within an range spanning several AMS-02 energy bins, such an excess signal can not be absorbed by the astrophysical background uncertainties. However, identifying the exact particle properties of the dark matter particle responsible for that excess is a a more model-dependent inquiry. Finally, in Sec. IV, we give our conclusions and discuss connections to other types of dark matter searches as well as future prospects.

II. METHODOLOGY

In this section, we describe the energy range of the AMS-02 positron fraction $[e^+/(e^+ + e^-)]$ measurement used in this analysis. We also explain how we construct our background astrophysical models, which are fitted to the AMS-02 positron fraction. We then describe the statistical analysis performed to set upper limits on dark matter particles annihilating, giving a contribution to the positron fraction. Finally, we construct positron fraction mock data based on the AMS-02 sensitivity to test whether a dark matter signal would be detectable; and how accurately we would be able to determine the dark matter mass, annihilation channel and cross section by our analysis.

We use astrophysical realizations created within Ref. [109], as a base to construct our background models for the positron fraction. We take the e^- and e^+ fluxes calculated from these realizations and add a dark matter contribution. Using these fluxes we perform fits, where we search for a potential dark matter component to the positron fraction and compute the 95% confidence level upper limits on the dark matter annihilation cross section as a function of mass. These fits are performed using a library of astrophysical/background realizations.

A. Cosmic-ray data

We use the recently published AMS-02 positron fraction measurement from [75,76] taken between May 2011 and November 2017. In Ref. [109], we found that the positron fraction spectrum sets stronger constraints on sources of cosmic-ray positrons, compared to the cosmic-ray positron flux spectrum. This is due to its smaller errors. Some systematic errors cancel when calculating cosmic-ray fractions versus cosmic-ray fluxes. We ignore the positron fraction measurement below 5 GeV, as that energy range is strongly affected by solar modulation and any dark matter annihilation signal from an approximately thermal relic would be hidden within the solar modulation

modeling uncertainties. Given that there is no publicly released covariance matrix by the AMS-02 Collaboration on that measurement, we treat the different energy bins as uncorrelated and add the systematic and statistical errors in quadrature.

B. Modeling the background to the dark matter contribution on the positron fraction

In this work, as signal we refer to a potential annihilating dark matter contribution on the positron fraction spectrum. As background we refer to all other astrophysical sources contributing to the positron fraction. Our modeling of the astrophysical background is based on Ref. [109]. These astrophysical realizations contain e^- fluxes from primary sources i.e., supernova remnants, secondary $e^\pm$ produced from inelastic collisions of primary cosmic ray nuclei with the ISM gas and $e^\pm$ from Milky Way pulsars. The main goal of Ref. [109], was to study the properties of Milky Way pulsars. Thus, a large number of astrophysical realizations was created. Those realizations accounted for a sequence of astrophysical uncertainties, as the stochastic nature of the neutron stars' birth in time and location, the stochasticity in the initial spin-down power of pulsars and their subsequent time evolution. Also Ref. [109], studied the fraction of pulsar spin-down power into cosmic-ray $e^\pm$ and how these injected cosmic rays propagate in the ISM and the Heliosphere.

In this work we start with the astrophysical/background realizations from Ref. [109] that were shown to be in good agreement with the *AMS-02* positron fraction [75,76], the e^+ flux [75,76], the total $e^+ + e^-$ flux [75,90], and also the total $e^+ + e^-$ fluxes from DAMPE [155] and CALET [148]. The quality of the fit is heavily impacted by the lowest energies of the positron fraction where the errors are the smallest. Adding a dark matter $e^\pm$ flux component that contributes at these low energies can drastically affect the quality of the fit. Thus, we include in our analysis astrophysical/background realizations from Ref. [109] that have a $\chi^2/n_{\rm dof} < 2.2$ in the positron fraction. This results in a total of 1020 astrophysical/background simulations, to account for all the background uncertainties. Some of those realizations in combination with a dark matter component may end up giving a much better quality of fit to the AMS-02 data and can explain the $e^\pm$ observations at energies where there is no contribution from dark matter.

For the dark matter contribution, we assume a local dark matter density of 0.4 GeV/cm^3 [6,8,9,156], set at 8.5 kiloparsec (kpc) from the galactic center. We take the dark matter halo in the Galaxy to follow a Navarro-Frenk-White (NFW) profile [157], with a characteristic radius of 20 kpc. We consider four simplified dark matter annihilation channels. These are: $\chi\chi \to e^+e^-$, $\chi\chi \to \mu^+\mu^-$, $\chi\chi \to \tau^+\tau^-$ and $\chi\chi \to b\bar{b}$. The annihilation cross section is set to be free in our analysis. We focus on low dark matter masses m_χ between 5 GeV and 50 GeV for the e^+e^- and the $\mu^+\mu^-$ channels, between 5 and 80 GeV for the $\tau^+\tau^-$ channel and between 10 GeV and 120 GeV for the $b\bar{b}$ one.

We calculate the injected $e^\pm$ production spectra from these dark matter annihilations using PPPC4DMID [158] and calculate the final e^- and e^+ spectra at the location of the Sun using GALPROP v54 [150,151]. The dark matter $e^\pm$ spectra are propagated through the ISM using the same 12 alternative propagation models as those defined in Table II of Ref. [109]. Every time that we test for a potential dark matter signal in the AMS-02 data, we make sure that the hypothetical dark matter $e^\pm$ flux, is evaluated under the same propagation conditions as its relevant astrophysical background. The 12 ISM models account for different choices on the thickness of the zone within which cosmic rays diffuse before escaping the Milky Way, how that diffusion depends on the cosmic-ray energy and finally for the energy losses of the cosmic-ray $e^\pm$ within the local volume of the Milky Way. This combination of ISM models encompasses the relevant astrophysical uncertainties within O(kpc) from the Sun [70,81,159]. For more details we refer the reader to Sec. II.E of Ref. [109]. In each astrophysical background, we add a dark matter contribution by choosing a specific annihilation channel and a specific mass and construct our final astrophysical + dark matter model. Given the different choices for the particle dark matter properties, we simulate 64 different combinations of annihilation channel and mass for each of the 1020 astrophysical backgrounds (65280 fits in total). The annihilation cross section is left as a free parameter to be set by the fit to the data. These final ISM e^- and e^+ spectra include the contribution of primary cosmic rays, secondary cosmic rays, cosmic rays from pulsars and from dark matter annihilations. We also propagate each of the ISM cosmic-ray spectra to the location of the Earth and account for solar modulation. That is done following the prescription of [160], where the modeling of the time, charge and energy dependence of solar modulation is accounted for by two fitting parameters, set within a range suggested by [161,162]. That same procedure was followed in Ref. [109]. The associated Bartels' Rotation numbers—relevant for the modeling of solar modulation effects—for the data-taking era are 2426-2514. Alternative approaches for the solar modulation of cosmic rays as they propagate within the Heliosphere exist; as for instance the numerical codes of HELMOD [163,164] and SOLARPROP [165] (see also [166–172]). Given the wide range for the values of the solar modulation fitting parameters (given in Table I), the exact treatment of solar modulation does not bias our results.

C. Statistical analysis

When we fit the astrophysical/background models to the *AMS-02* positron fraction we have seven parameters. These account for the cosmic-ray primary e^- flux, the secondary $e^\pm$ flux and the pulsar $e^\pm$ flux normalizations, that each has

their own uncertainty (see e.g., [173]). We include two parameters to allow for a spectral softening/hardening of the cosmic-ray primary and secondary spectra; and two more for the solar modulation modeling. Once adding the dark matter component we have an additional (eighth) parameter, that is directly proportional to the fitted annihilation cross section. For a given astrophysical background, once adding a potential dark matter component in the fitting procedure, we allowed the other seven parameters to be free within 50% of their best-fit value achieved in the background only fit. In Appendix A we give the full parameter space tested in our astrophysical and dark matter models and its subsequent minimization procedure.

We perform a χ^2 minimization, and use a combination of SciPy's [174] LEAST_SQUARES routine from the OPTIMIZE module and IMINUIT [175,176]. We found that the fastest minimization is achieved by performing a few minimization steps with the LEAST_SQUARES routine with high tolerance and finishing the minimization with IMINUIT.

In Fig. 1, we show the fit to the positron fraction for one of our background models with a dark matter component included. For the dark matter we have taken, $m_\chi = 25$ GeV and the annihilation channel to be $\chi\chi \to b\bar{b}$. One can see all the relevant contributions from primary e^-, secondary e^+, pulsar e^+, and e^+ originating from dark matter. The background only hypothesis gave for this model a $\chi^2_{\rm DM=0}/n_{\rm dof} = 2.11$; while after including dark matter we got a $\chi^2_{\rm DM}/n_{\rm dof} = 1.15$. $n_{\rm dof}$ is the number of degrees of freedom. The pull of the fit, which is $({\rm data} - {\rm model})/\sigma_{\rm data}$ is also shown at the bottom of the figure.

The dark matter mass range that we study in this work, contributes at the lower energies and has no effect on the higher energies where the spectrum is dominated by the local pulsar population. Also, other than the $\chi\chi \to e^+e^-$ annihilation channel, the dark matter component cannot produce sharp peaks in the positron fraction that could explain features like the one we identified in Ref. [109] and studied in Ref. [177] at ~ 12 GeV. We find that statement to be true for every astrophysical/background model. Moreover, we note that the treatment of solar modulation can not cause sharp spectral features as the 12 GeV one, which spans only five AMS-02 data points or equivalently an energy range of approximately 3 GeV.

In order to derive upper limits on the dark matter annihilation cross section, presented as $\langle\sigma v\rangle$, we use a likelihood ratio test. The null hypothesis is that there is no dark matter contribution and we just have the astrophysical background, i.e., seven fitting parameters with $\langle\sigma v\rangle = 0$. The alternative hypothesis is that there is some contribution from dark matter annihilation with annihilation cross section (times velocity, thermally averaged) $\langle\sigma v\rangle$, i.e., eight fitting parameters. We rely on Wilks' theorem [178], and use the statistic $LR = -2\log\Lambda(=\chi^2$ difference), with Λ the likelihood ratio of the null (background only) hypothesis over the alternative dark matter + background hypothesis. This is distributed according to a χ^2_ν-distribution with ν degrees of freedom, where ν is the difference of fitting parameters between the two hypotheses models. In our case, we have $\nu = 1$. However, that would give a naive estimate of the p-value since the null hypothesis corresponds to the case $\langle\sigma v\rangle = 0$, i.e., it lies on a boundary of our parameter space. This problem can be overcome by using Chernoff's theorem [179]. The LR follows a $\frac{1}{2}\delta(x) + \frac{1}{2}\chi^2$ distribution (half chi-square distribution) with one degree of freedom [180]. This means that the p-value is reduced by half compared to the naive estimate.

Following the standard convention in the literature, we can deduce 95% upper limits on $\langle\sigma v\rangle$ for each astrophysical background at a fixed annihilation channel and dark matter mass. This is done by scanning over $\langle\sigma v\rangle$, computing the χ^2 profile and finding at which value of $\langle\sigma v\rangle$ we have $\chi^2_{\rm DM} = \chi^2_{\rm DM=0} + 2.71$. This corresponds to the 95% upper limit of a half chi-square distribution with one degree of freedom. Because we have multiple masses, we essentially have a 2D grid of masses and cross sections where we compute the χ^2 profile and draw the contour where the $\chi^2_{\rm DM}$ increased by 2.71 from $\chi^2_{\rm DM=0}$. At each point of the grid the rest of the background nuisance parameters are optimized such that the χ^2 is minimum. This contour is the 95% upper limit on the dark matter annihilation cross section as a function of the mass. This can be done for each annihilation channel and for each pulsar background, resulting in each background giving a different upper limit. We report the combination of those upper limits.

D. Mock data

In this paper, we produce mock data of the AMS-02 positron fraction. We do that to test whether a dark matter contribution in the positron fraction would be detectable and with its properties (mass, annihilation cross section and channel) correctly identified. We produce these mock data by taking existing backgrounds and adding a flux component from dark matter of specific mass, annihilation channel and cross section. We then calculate the positron fraction spectra that the AMS-02 would observe. These mock spectra include only statistical errors. We treat these mock spectra as we treated the AMS-02 measurement and scan them with our background + dark matter models to see if we can recover the original mass, annihilation channel and cross section. By keeping only the statistical errors we are optimistic on the ability of the positron fraction measurement to help us probe the properties of a dark matter signal.

For the mock positron fraction spectra we use two annihilation channels: $\chi\chi \to \mu^+\mu^-$ and $\chi\chi \to \tau^+\tau^-$, and

test four dark matter mass and annihilation cross section combinations. For the $\chi\chi \to \mu^+\mu^-$ channel we have

(a) $m_\chi = 15$ GeV and $\langle\sigma v\rangle = 2 \times 10^{-26}$ cm^3 s^{-1},
(b) $m_\chi = 15$ GeV and $\langle\sigma v\rangle = 5 \times 10^{-27}$ cm^3 s^{-1},
(c) $m_\chi = 30$ GeV and $\langle\sigma v\rangle = 2 \times 10^{-27}$ cm^3 s^{-1},
(d) $m_\chi = 30$ GeV and $\langle\sigma v\rangle = 5 \times 10^{-28}$ cm^3 s^{-1}.

For the $\chi\chi \to \tau^+\tau^-$ channel we have

(a) $m_\chi = 15$ GeV and $\langle\sigma v\rangle = 1 \times 10^{-25}$ cm^3 s^{-1},
(b) $m_\chi = 15$ GeV and $\langle\sigma v\rangle = 2 \times 10^{-26}$ cm^3 s^{-1},
(c) $m_\chi = 30$ GeV and $\langle\sigma v\rangle = 2.5 \times 10^{-26}$ cm^3 s^{-1},
(d) $m_\chi = 30$ GeV and $\langle\sigma v\rangle = 5 \times 10^{-27}$ cm^3 s^{-1}.

We use two astrophysical backgrounds to create these mock data, one for each channel. These two backgrounds are in agreement with the AMS-02 e^+ flux, positron fraction and total $e^+ + e^-$ flux measurements, and also with the DAMPE and CALET total $e^+ + e^-$ flux measurements.

In Fig. 2, we show an example of such a mock positron fraction where there is a contribution from 30 GeV dark matter particles annihilating to $\tau^+\tau^-$ with an cross section of $\langle\sigma v\rangle = 5 \times 10^{-27}$ cm^3 s^{-1}. We also show a fit to that mock positron fraction by one of our models and the original *AMS-02* data with a fainter color for comparison to the mock ones. The errors of the mock positron fraction are much smaller as we only consider statistical uncertainties.

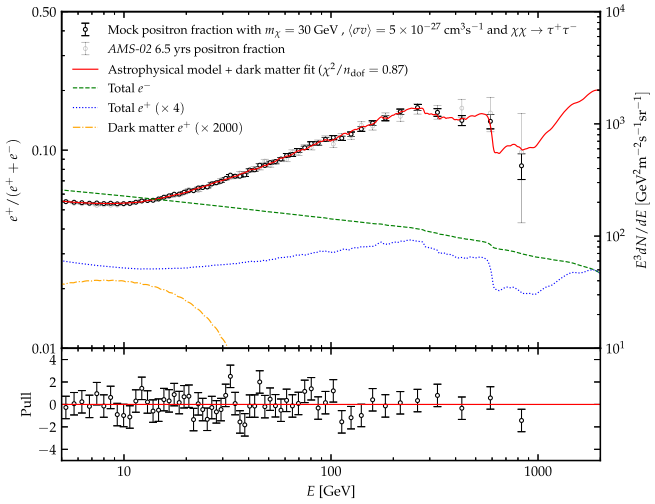

FIG. 2. A mock positron fraction created by the combination of an astrophysical background with a dark matter signal. We chose an astrophysical background that without the dark matter contribution gave a good fit to the positron fraction ($\chi^2/n_{\rm dof} = 1.14$). We add the contribution from a 30 GeV dark matter particle that annihilates to $\tau^+\tau^-$ with a cross section of $\langle\sigma v\rangle = 5 \times 10^{-27}$ cm^3 s^{-1}. We show an astrophysical background + dark matter model fit to the mock positron fraction and also the total e^-, e^+ and e^+ originating from dark matter fluxes within that model in the green dashed, blue dotted and orange dash-dotted lines with the units provided by the right y-axis. At the bottom, we show the pull distribution of the fit. We also show with faint gray the real AMS-02 positron fraction measurements.

Once a mock positron fraction spectrum that includes a dark matter component is created, we test our ability to deduce the particle dark matter properties. We scan the mock positron fraction spectra, by testing the combination of 100 backgrounds (including the backgrounds used to create them) with all the 64 combinations for the dark matter annihilation channel and mass used.

III. RESULTS

A. Upper limits on the dark matter annihilation cross section

For a given astrophysical background and after fixing the annihilation channel and dark matter mass m_χ, we can calculate a unique limit of the dark matter annihilation cross section. In this work we show results for the annihilation cross section times the relative dark matter particles' velocity $\langle\sigma v\rangle$ (thermally averaged). In Fig. 3, we show for the m_χ versus $\langle\sigma v\rangle$ parameter space the quality of χ^2 fits as "heatmaps", for the four annihilation channels that we study. In each case these are evaluated by fixing the astrophysical background to be one out of the 1020 that we use as a basis to account for astrophysical modeling uncertainties. As we have explained in Sec. II C, we allow for eight fitting parameters. In these heatmaps the $\Delta\chi^2$ is evaluated from the case of no dark matter annihilation (i.e., $\langle\sigma v\rangle = 0$). Points with negative $\Delta\chi^2$, (given in different shades of blue) represent dark matter assumptions for which we get a better fit to the positron fraction than without a dark matter contribution. Instead, points with positive $\Delta\chi^2$, (given in different shades of red) represent dark matter assumptions that are statistically excluded by the positron fraction data. Our discretized parameter space shows the grid points that we used to probe the m_χ versus $\langle\sigma v\rangle$ parameter space.

As can be seen from Fig. 3, for each channel and for the specific astrophysical backgrounds shown, there is a strong preference for a dark matter contribution to the positron fraction. This is shown by the dark blue ranges around which we evaluate the best fit m_χ and $\langle\sigma v\rangle$ parameter point and the 1, 2, and 3σ signal significance contours. We also show the 95% upper limit on $\langle\sigma v\rangle$ as a function of m_χ (in the solid black lines).[2] However, what is shown in Fig. 3 represents only the results coming from one background for each of the four channels. We find that both the 95% upper limits and the excess contours depend on the exact astrophysical background used. That statement is true for all channels studied and for a wide range of masses.

We discuss first the impact that alternative astrophysical background assumptions have on the upper limits to the

[2]These upper limit lines are only exact at the centers of our mass "bins". It shouldn't be worrying that the line goes over areas of negative $\Delta\chi^2$ (blue) since the algorithm tries to interpolate in the mass range between our mass "bins".

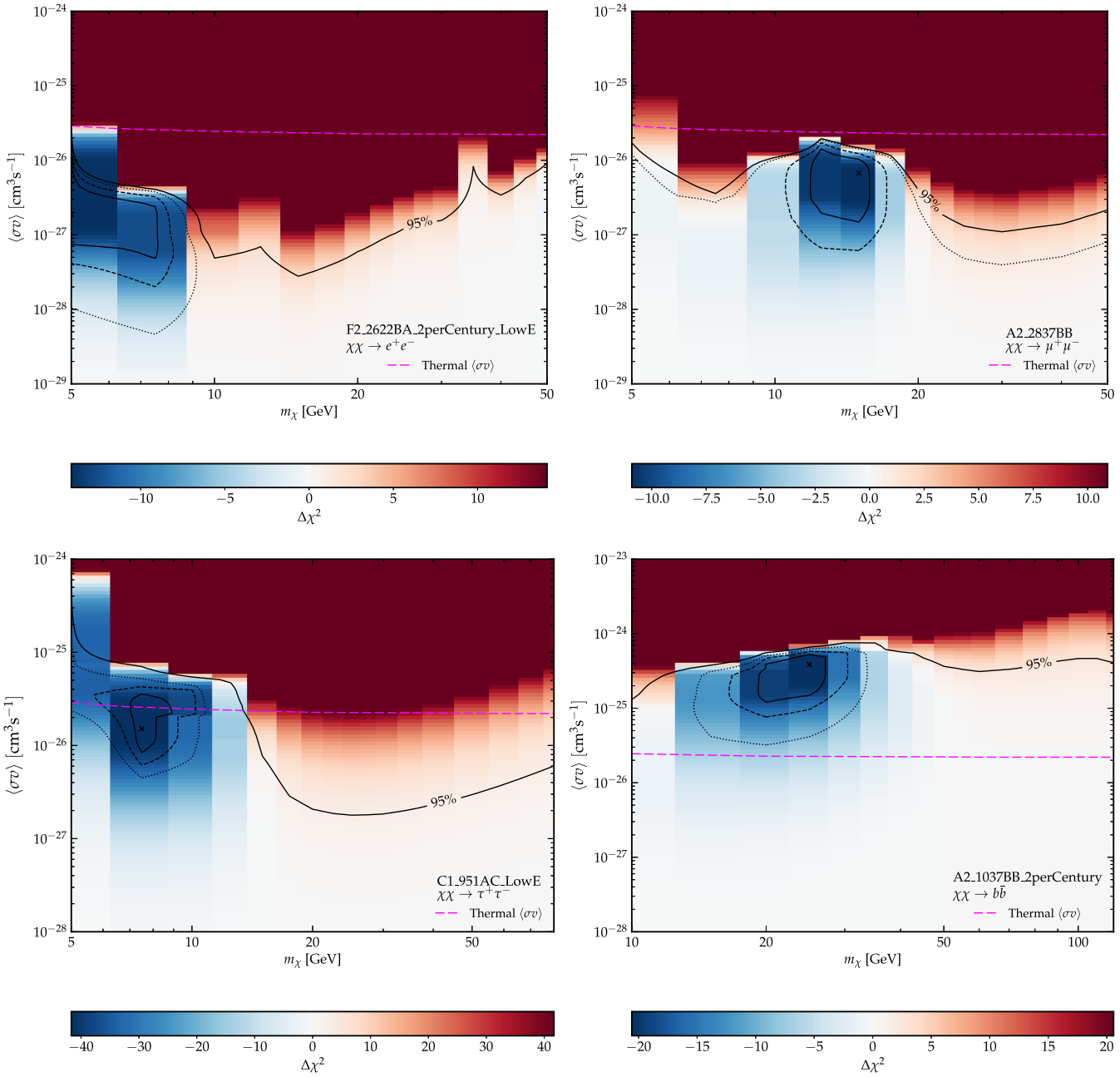

FIG. 3. The χ^2 profiles presented as heatmaps for four different astrophysical backgrounds with the addition of dark matter annihilating to e^+e^- (upper left), $\mu^+\mu^-$ (upper right), $\tau^+\tau^-$ (lower left) and $b\bar{b}$ (lower right). In each heatmap we mark the best fit point with an "x" and draw the 1σ (solid), 2σ (dashed) and 3σ (dotted) contours around the best fit point. In the colorbars we show the $\Delta\chi^2$ values from fitting just the astrophysical background without the addition of annihilating dark matter. We also show the 95% upper limit lines on $\langle\sigma v\rangle$ for each one of these four backgrounds as constructed in Sec. II C. Finally, the dashed magenta lines are the expected $\langle\sigma v\rangle$ for a thermal relic from Ref. [55]. The left two plots are with low-energy extrapolated backgrounds while the right two ignore the low-energy extrapolation (see text for details and also Ref. [109]).

dark matter cross section. By exploring the parameter space we have found that models with similar assumptions for the combination of energy losses and diffusion end up giving similar upper limits and excess regions in each annihilation channel and type of background (low-energy extrapolated or not). That is especially true for the energy losses in agreement with [82]. Changing the assumptions on the ISM energy loss rate, does not dramatically change the shape of

the dark matter $e^{\pm}$ spectra in the energy ranges that we fit.[3] However, it does affect the amplitude of these fluxes for a given mass, cross section and channel. Lower energy losses allow for the observed $e^{\pm}$ of dark matter origin to be sourced from a wider volume of the local Milky Way. Thus, the dark matter $e^{\pm}$ flux that reaches us is higher when we assume lower-energy losses; setting in turn tighter limits on the allowed dark matter annihilation cross section. Lower ISM energy-loss rates enhance in amplitude the background astrophysical flux components as well. Yet, that enhancement in those fluxes' amplitude is absorbed in our analysis as part of the uncertainty in the efficiency of the underlying background sources, i.e., the assumptions on the SNRs, pulsars and the ISM gas density. Thus changing the energy-loss rate assumptions has a residual effect only on the annihilation cross section limits. Instead, the assumptions about how fast cosmic rays diffuse have a much smaller impact on the final dark matter limits. Similarly, the assumptions of the galactic scale-height have a very small effect on the cross section upper limits. For a given dark matter model's propagated $e^{\pm}$ spectrum, the lower the observed energy is, the larger the volume of origin of those $e^{\pm}$ within the Milky Way. For the dark matter masses we focus here, different choices on the diffusion coefficient, diffusion index and scale height affect mostly the propagated spectra at energies below ~ 5 GeV, that we do not fit due to the large solar modulation modeling uncertainties. The effects of different diffusion assumptions on the background fluxes are important if one fixes all other modeling assumptions; but once marginalizing over the rest of those assumptions, the diffusion has a small effect on how much room there is for an additional dark matter $e^{\pm}$ flux component.

Having created heatmaps as those of Fig. 3, testing the variety of alternative astrophysical assumptions we concluded that instead of using the entire library of 1020 astrophysical background assumptions we can reduce our analysis to a sample of 60 astrophysical background models for each annihilation channel (there is some overlap between channels). All of these 60 backgrounds are within 2σ from a $\chi^2/n_{\rm dof} = 1$ after including dark matter at their best fit point. Combining different upper limit lines from different backgrounds for the same channel, we construct upper limit bands. In Fig. 4, we show these upper limit bands for our four annihilation channels evaluated from our 60 astrophysical background models per dark matter channel.

[3]For masses $m_\chi \sim 50$ GeV and for propagated $e^{\pm}$ of energy up to 5 GeV, the spectral shapes of the dark matter fluxes studied here change very little by varying the ISM conditions. At energies lower than ~ 5 GeV, lower energy losses make the dark matter spectrum at Earth harder. Given that we focus on relatively light dark matter, alternative choices on the ISM energy losses have little impact in the spectral shape (excluding the normalization) of the dark matter originated fluxes.

The 60 background models include the probed range of local energy losses, the alternative choices for the Milky Way's local diffusion properties, as well as alternative assumptions for the pulsars' flux component at energies of $O(10)$ GeV. The energy-loss assumptions affect mostly the $e^{\pm}$ fluxes of the dark matter component at energies close to the dark matter mass m_χ. As the leptonic channels give dark matter fluxes to $e^{\pm}$ that are harder in spectrum than the primary e^- and secondary $e^{\pm}$ astrophysical components, the dark matter component becomes most important in relevant terms at energies close to $\sim m_\chi$. As we explained earlier, alternative choices for energy losses (and to a smaller extend diffusion) affect that energy range where for a given mass and annihilation channel the dark matter flux becomes most relevant. The alternative choices on the pulsars' flux component at energies of $O(10)$ GeV are relevant here for the dark matter masses that we study. At $O(10)$ GeV many old and distant pulsars contribute and as a result their contribution depends on a larger number of assumptions than the contribution of local and younger pulsars at higher $e^{\pm}$ energies. We represent that by breaking our results in Fig. 4, into models "with low-energy extrapolation" and models "without low-energy extrapolation". The low-energy extrapolation backgrounds give a higher flux from distant and older pulsars. The cosmic-ray measurements from AMS-02, CALET and DAMPE probe best the pulsars' contribution at high energies. Thus, using a range of assumptions that result in a wider range of predictions on the more uncertain low-energy astrophysical $e^{\pm}$ background, is the conservative way to set limits on annihilating dark matter particles with mass of 5–50 GeV. In the 60 backgrounds we make sure to include 30 of the best-fit models from Ref. [109], where the full parameter space of local Milky Way properties was probed and models for which after adding the dark matter component we get high quality fits to the data.

In Fig. 4, there is a rough order in the values of the annihilation cross section limits. Our fits show that there is preference for a higher $\langle \sigma v \rangle$ when we use $b\bar{b}$ as our channel, followed by $\tau^+\tau^-$, followed by $\mu^+\mu^-$ and then e^+e^-. That is to be expected as the annihilation channels to more massive Standard Model particles give $e^{\pm}$ fluxes that span a wider range and have less prominent spectral features. This makes the dark matter $e^{\pm}$ fluxes easier to conceal within the background fluxes and their modeling uncertainty.

Another result, is that for the three leptonic channels the backgrounds with the low-energy extrapolated pulsars' flux prefer smaller dark matter masses of the order of 5–10 GeV, while the backgrounds without the low-energy extrapolation generally prefer higher masses. Following, we explain first the lower masses results. Backgrounds with low-energy extrapolation have a higher flux originating from

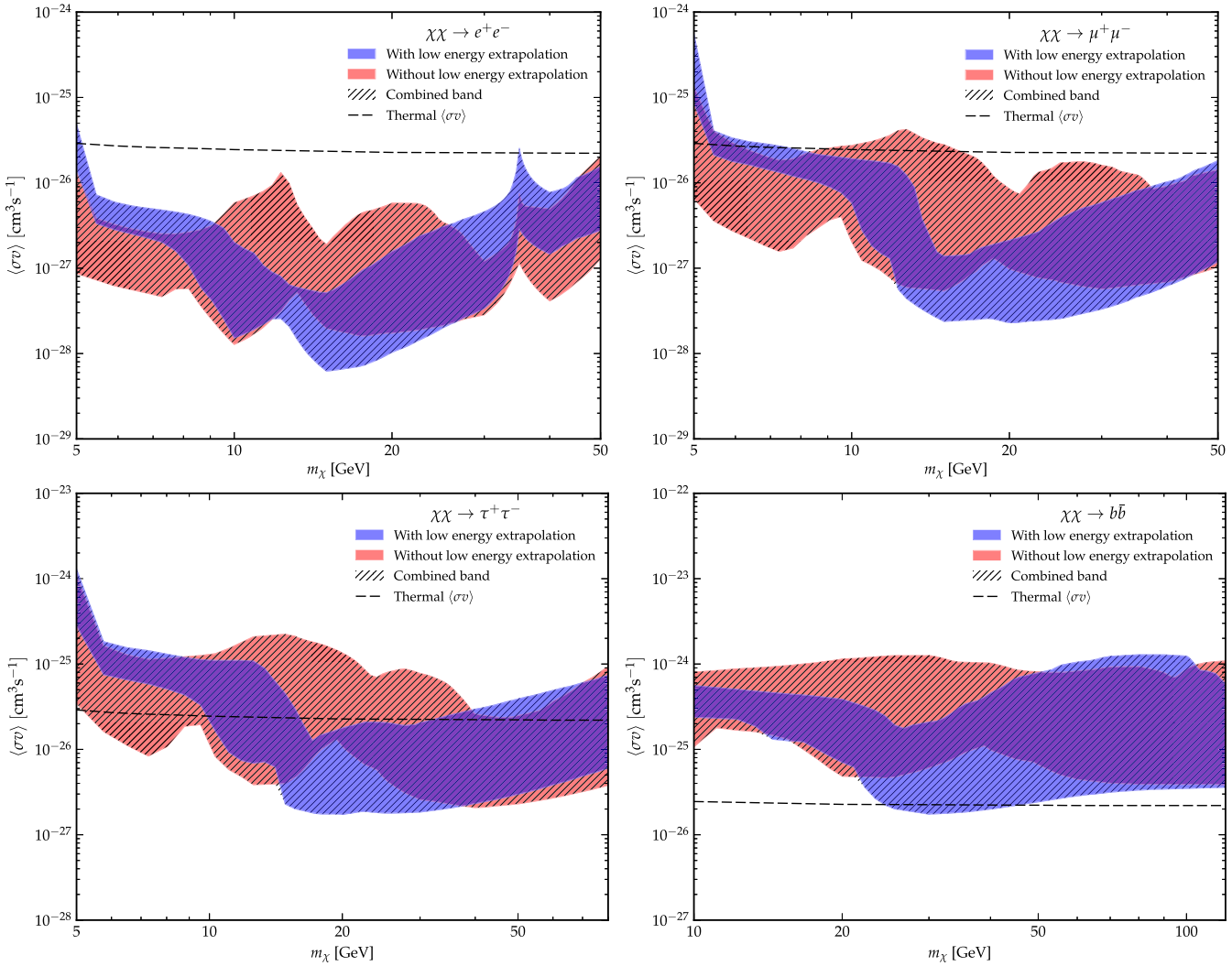

FIG. 4. The 95% upper limit bands on the annihilation cross section $\langle\sigma v\rangle$ to $e^+ + e^-$ (upper left), $\mu^+\mu^-$ (upper right), $\tau^+\tau^-$ (lower left) and $b\bar{b}$ (lower right), each from 60 astrophysical backgrounds that sufficiently cover the astrophysical backgrounds parameter space. We separate the bands that come from backgrounds with (blue) and without (red) low-energy extrapolation and also show the combined band (hatched). The dashed lines are the expected $\langle\sigma v\rangle$ for a thermal relic taken from Ref. [55].

pulsars at energies $\lesssim O(10)$ GeV.[4] In our multidimensional parameter space minimization, when pulsars predict a higher flux at low energies, the positron fraction is fitted better by a higher flux from dark matter as well. That counter intuitive statement is due to the large impact the first few positron fraction data points (at 5–10 GeV) have on the fit. We remind that the positron fraction error bars at those energies are the smallest (see Fig. 1). At those low energies, the secondary positrons provide a prominent flux component. The secondary cosmic-ray modeling assumptions together with those on solar modulation dominate the fit between 5 and 10 GeV. Changing the pulsars' flux assumptions at energies bellow $O(10)$ GeV impacts the secondary positrons and electrons spectra in the entire energy range of the observed positron fraction. The impact of this on the dark matter limits is shown in Fig. 4. Backgrounds with a higher pulsar $e^\pm$ flux prediction at low energies result also in more room for a *localized in energy* dark matter signal. Again the "with low-energy extrapolation" backgrounds, predict a higher $e^\pm$ flux from pulsars at energies $\lesssim$O(10) GeV to the "without low-energy extrapolation". For the leptonic channels, that give $e^\pm$ flux that peaks in a small energy range as is especially the case with the $\chi\chi \to e^+e^-$ and $\chi\chi \to \mu^+\mu^-$ channels the low-energy extrapolation backgrounds usually give weaker limits. We note that for the $\chi\chi \to b\bar{b}$ channel, the situation is different as the dark matter flux spans a wide energy range.

[4]We write at $E \lesssim O(10)$ GeV, instead of $E \lesssim 10$ GeV, as the low-energy extrapolation that we use for the modeled pulsar $e^\pm$ flux starts at energies anywhere between 10 GeV and 30 GeV depending on modeling assumptions.

The cosmic-ray positron fraction has three spectral features around 12, 21, and 48 GeV that were identified to be prominent in Refs. [109,177]. For the $\chi\chi \to e^+e^-$ channel, the lower two in energy features have an effect on our limits. This annihilation channel gives a dark matter $e^\pm$ flux with a sharp break at energy $E \lesssim m_\chi$. For the backgrounds without the low-energy extrapolation we see three mass regions at $m_\chi = 10$–12 GeV, at $m_\chi \sim 20$ GeV and at $m_\chi \sim 35$ GeV where the limits are weaker. Dark matter particles with mass of 10–12 GeV, give cosmic-ray $e^\pm$ with energies lower than 12 GeV. Thus, their limits are not directly affected by the 12 GeV positron fraction feature. The weakest limits for that mass range are created by backgrounds with enhanced local ISM energy losses. The weak limits for the mass region of $m_\chi \sim 20$ GeV are associated to the 12 GeV feature of the positron fraction measurement and are derived from ISM backgrounds with conventional local ISM energy losses. The weaker limits at $m_\chi \sim 35$ GeV, are associated to the 21 GeV feature on the positron fraction. Both the blue and red shaded regions find weaker $\langle\sigma v\rangle$ limits for $m_\chi \sim 35$ GeV, as around 20 GeV in $e^\pm$ cosmic-ray energy their background predictions are similar.

For the annihilation channel to $\mu^+\mu^-$, the upper limit bands show two mass ranges where the limits become weak, at $m_\chi 10$–15 GeV and at $m_\chi \sim 30$ GeV. Again, the first mass range is not affected by the presence of the positron fraction spectral features. The weakest limits for the 10–15 GeV mass range come from ISM models of increased local energy losses and for the "without low-energy extrapolation" background assumption. The weaker limits for $m_\chi \sim 30$ GeV, originate from the 12 GeV feature. The 21 GeV feature has an effect on the highest end of the shown mass range

For the annihilation channel to $\tau^+\tau^-$, the upper-limit bands become weak, in the wide mass range of $m_\chi 10 - 40$ GeV. This is similar to what was described for the $\chi\chi \to \mu^+\mu^-$ channel. However, what was two mass ranges for the $\mu^+\mu^-$ has merged into one. The $\tau^+\tau^-$, has a dark matter $e^\pm$ spectrum less localized in energy than the $\mu^+\mu^-$.

For the $\chi\chi \to b\bar{b}$ channel, the limits for backgrounds without the low-energy extrapolation to the pulsars' component are almost always weaker for masses $m_\chi < 50$ GeV. As we said the $b\bar{b}$ channel gives a cosmic-ray $e^\pm$ flux that spans a wide range. Thus, a suppressed background positron flux allows for weaker constraints on the dark matter contribution to the positron fraction. For the $b\bar{b}$ channel and for mass m_χ of 50–120 GeV, the limits are roughly the same for the backgrounds with or without the low-energy extrapolation. For these higher masses the dark matter originated $e^\pm$ flux is prominent above the energy range where the extrapolation is used.

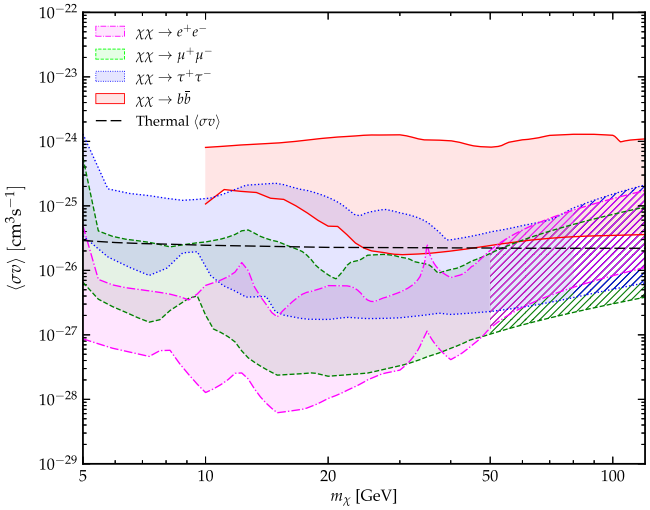

FIG. 5. The combined 95% upper limit bands on $\langle\sigma v\rangle$ for our four different annihilation channels. The e^+e^-, $\mu^+\mu^-$ and $\tau^+\tau^-$ channel bands are extrapolated up to 120 GeV to match the higher end of the $b\bar{b}$ channel mass range. The extrapolated regions are shown hatched. The black dashed line is the expected $\langle\sigma v\rangle$ for a thermal relic from Ref. [55].

In each one of the plots of Fig. 4 we also have the combined band with and without low-energy extrapolation as a hatched region. In Fig. 5, we show the four combined upper limit bands, one for each of our annihilation channels where we have also extrapolated those bands up to 120 GeV where necessary. We claim at this point that the upper limits on $\langle\sigma v\rangle$ from the cosmic-ray positron fraction, are much more uncertain than previously claimed. Due to the uncertainties in the astrophysical backgrounds including the pulsar component, there isn't a well defined upper limit line. Instead, we present upper limit bands evaluated from a collection of viable astrophysical backgrounds, that each gives a different upper limit line. Our bands at certain masses can span up to two orders of magnitude in the constrained parameter $\langle\sigma v\rangle$, as e.g., for $\chi\chi \to \mu^+\mu^-$ with $m_\chi = 15$ GeV.

B. A possible excess flux of low cosmic-ray energy positrons

As we show in Fig. 3, for the specific background astrophysical model used, we can find combinations of dark matter mass, annihilation cross section and channel, where there is a significant statistical preference for an additional dark matter component. In that example, the fit to the positron fraction improves by a $\Delta\chi^2$ of up to 40. The most statistically significant result comes from a $\chi\chi \to \tau^+\tau^-$ with $m_\chi = 7.5$ GeV and $\langle\sigma v\rangle \simeq 1.5 \times 10^{-26}$ cm^3 s^{-1}. Such a dark matter particle, has similar properties to those required to explain the galactic center excess in gamma rays [59–70].

In this subsection, we further pursue this indication of a possible dark matter component. We test whether this is a result of just a specific combination of astrophysical background assumptions, or a result that stands to further scrutiny once we allow for a wide range of astrophysical backgrounds. We use the set of 60 astrophysical background models with all the seven astrophysical nuisance parameters plus the one related to the dark matter annihilation cross section as we described in Sec. II C.

In Fig. 6, we show in a similar manner to Fig. 4, the 2σ excess contour regions for our four dark matter annihilation channels. There are 60 overlaid contour regions in each plot. These excess regions are in agreement with our upper limit bands. The respective upper limits like the ones presented in Fig. 3 for a specific background, get weaker when the excess contours suggest a high annihilation cross section. Some isolated islands in the cross section versus mass space are also observed. These are created by very few background models and are typically of minor statistical significance. In fact, we find that for some of the backgrounds used, while there still is some improvement by adding a dark matter component, that is a small one. In particular, for 2 out of the 60 background models, by adding dark matter annihilating to e^+e^-, or $\mu^+\mu^-$, or $\tau^+\tau^-$ leptons the improvement in $\Delta\chi^2$ is less than 6. That results in open 2σ contours depicted by light red or blue regions extending to effectively zero annihilation cross sections. For dark matter particles annihilating to $b\bar{b}$, there are 6 out of the 60 backgrounds where that is the case. This shows that this "excess" is not always statistically significant. However, we note that for most of the tested backgrounds there is some excess $e^{\pm}$ flux compatible to that coming from locally annihilating dark matter. As we will explain in detail in Sec. III C, even if indeed this is a dark matter signal, deducing its particle properties is highly

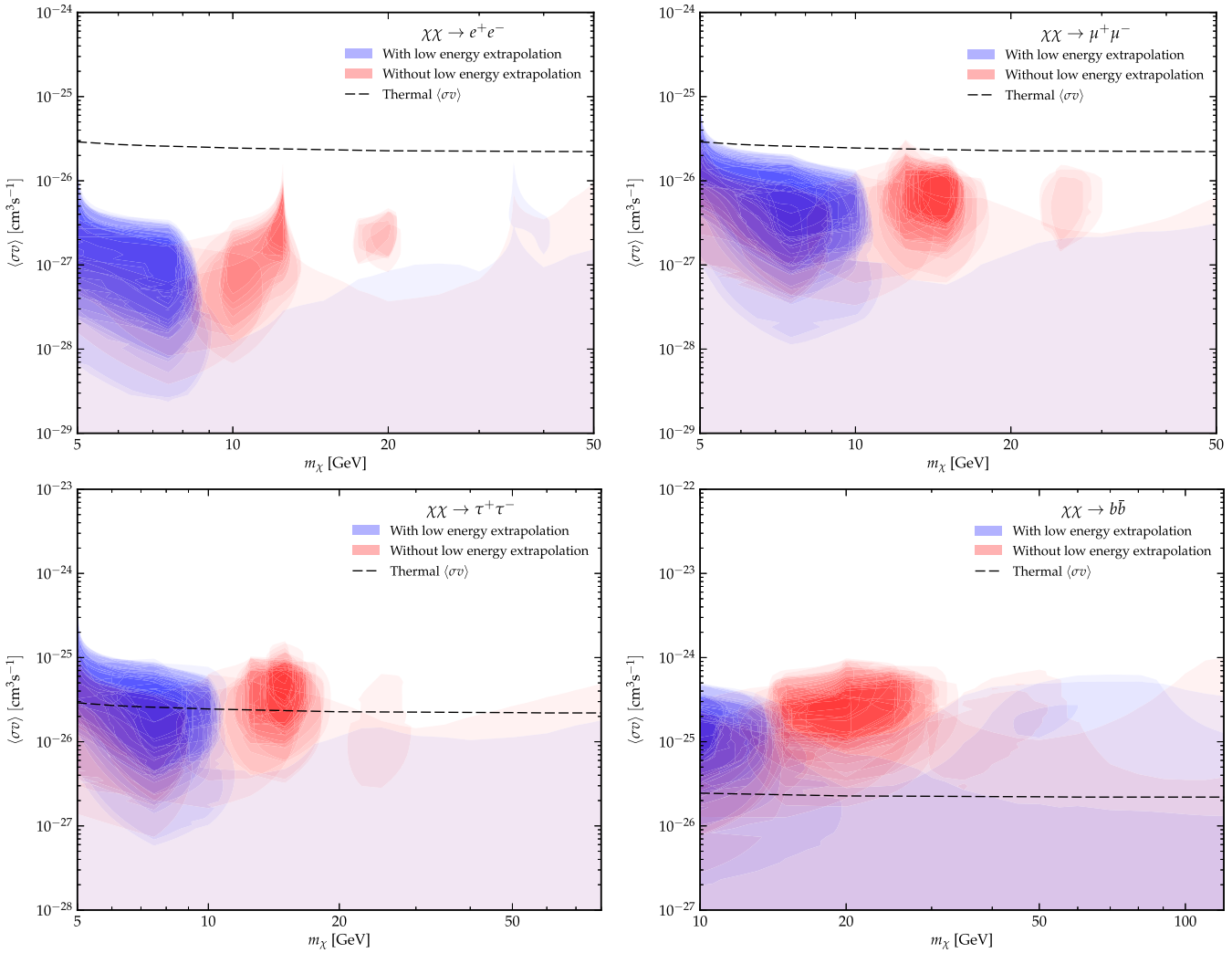

FIG. 6. In a similar manner to Fig. 4, we show the 2σ excess contour regions for the dark matter annihilation cross section versus mass. The dashed lines are the expected $\langle\sigma v\rangle$ for a thermal relic taken from Ref. [55].

challenging. Also, we note that some of the parameter space suggested by the excess is excluded by limits from the cosmic microwave background, gamma rays and antiprotons [17,73,181].

We can not claim and do not claim any robust $e^{\pm}$ excess flux between 5 GeV and 15 GeV on the positron fraction spectrum. We just note that we used background models that always agree with higher-energy $e^{\pm}$ observations from AMS-02, CALET and DAMPE, and that half of the 60 astrophysical background models give (without a dark matter component) a good quality fit of $\chi^2/n_{\rm dof} < 1.3$ to the positron fraction from 5 GeV to 1 TeV. Yet, a $> 2\sigma$ excess for the low-energy cosmic-ray $e^{\pm}$ flux is found for the great majority of these background models. We also find a tendency for background models with high local-energy losses, of $dE/dt \sim 8 \times 10^{-6}$ GeV^{-1} kyr$^{-1}(E/(1\ \text{GeV}))^2$, to reduce the significance for that excess component. Further understanding of the astrophysical, nuclear and particle physics uncertainties at the 1–20 GeV cosmic-ray energy range is needed to more accurately model the primary and secondary production of cosmic rays, as well as constrain better their propagation properties through the ISM and the Heliosphere. Finally, having a full knowledge of the correlated errors on the positron fraction measurement will be of great benefit to elucidate the *AMS-02* observations. In the absence of such a published result by the AMS-02 Collaboration, we leave this issue of a possible $e^{\pm}$ "excess" flux an open question.

C. Ability to detect dark matter in the AMS-02 positron fraction measurement

In this section, we check if the AMS-02 positron fraction measurement can be used to probe the properties of a dark matter component in it. As we describe in Sec. II D, we use eight combinations of dark matter mass, annihilation cross section and channel to create mock positron fraction measurements. These mock positron fraction measurements take also into account the flux predictions from one specific background per annihilation channel. These two backgrounds were selected to provide a good fit to the AMS-02, CALET and DAMPE cosmic-ray lepton measurements (see Ref. [109]).

We test these mock observations by searching for a dark matter signal. We first want to test if by adding an excess signal of dark matter origin we can at the very least identify its presence, i.e., the presence of an additional term that doesn't come from cosmic-ray primaries, secondaries or the main population of local pulsars. That does not exclude that an excess flux in low-energy positrons can still be of a more conventional astrophysical origin as e.g., a collection of very powerful, nearly simultaneous but old supernova remnants giving a high flux of $e^{\pm}$ in that range [118], or a similar collection of very (and atypically) powerful pulsars, or $e^{\pm}$ from cosmic-ray activity in the center of the Milky Way [177]. As a second level question, we want to see if assuming that excess term is of dark matter origin, whether we can identify its specific particle physics properties (mass, annihilation channel and cross section).

We fit each one out of the eight mock data by being agnostic to both the background and the dark matter signal. We test all combinations of 100 backgrounds and all dark matter channels and masses (64 in total). Thus we perform 6400×8 such fits. We check whether the combinations of background & dark matter channels and masses that were used to create the mock data are statistically significant against the other combinations. We remind the reader that the annihilation cross section is let to be free in our fitting procedure. We find that the astrophysical background is easily identifiable i.e., we can find which one out of the 100 backgrounds was used to create the mock positron fraction. We also find that we can at the very least identify the presence of an additional term contributing to the positron fraction, i.e., a nonzero annihilation cross section. When fitting to mock data that originated from a particular astrophysical background, all the good fits found are combinations of that background + some dark matter contribution. However, the properties of that dark matter component are not easily identifiable. As the astrophysical background dominates the positron measurement in the entire energy range it is possible to pick out the underlying background model used to create the mock data. That is not the case with the dark matter component that affects the measurement only in a narrow energy range.

The dark matter annihilation channel is very challenging to identify. After scanning our mock data, we find that there is no statistical significance for models that are built with the original dark matter annihilation channel over the other three channels. Among the best fits to each mock data, the fit doesn't give any preference between different annihilation channels. Even if a dark matter signal is present within cosmic-ray $e^{\pm}$, we cannot identify the annihilation channel that produces that signal. For that reason, we perform an additional test where we fix the dark matter annihilation channel to the one used to create each of our mock data.

In Fig. 7, we show the results of scanning our mock data with only the channels that were used to create them. On the left we show the results for the $\chi\chi \to \mu^+\mu^-$ mock data and on the right the results for the $\chi\chi \to \tau^+\tau^-$ mock data. For each one of these eight cases we test a combination of 100 backgrounds $\times 17$ masses. The maximum number of empty markers that could exist for each type is 1700. Those that appear in the plots are the ones within 2σ of a $\chi^2/n_{\rm dof} = 1$, which means $\chi^2/n_{\rm dof} \leq 1.31$. If small clusters of similar empty markers (best-fit points) form around the same filled markers (original mock data parameters), then this points to our ability to correctly identify the dark matter properties using the positron fraction. We stress that for these results, we are not being agnostic about the

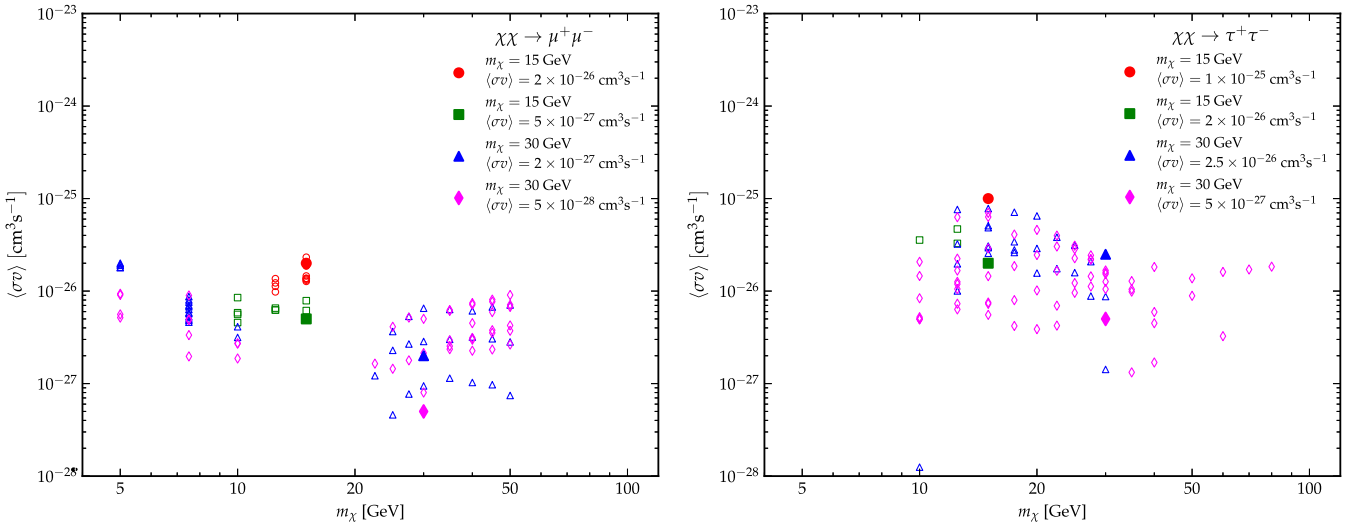

FIG. 7. Scatter plots of best fit points in our 2D dark matter parameter space of the backgrounds + dark matter models that are within 2σ of a $\chi^2/n_{\rm dof} = 1$. We show results derived after scanning the mock data testing only the same dark matter channel to the one used to create them. On the left, we show the results for the $\chi\chi \to \mu^+\mu^-$ mock data, while on the right, we show the results for the $\chi\chi \to \tau^+\tau^-$. With filled larger markers we denote the original points, i.e., the dark matter properties that we used to create the mock data. With the smaller empty markers of the same style, we denote the best fit points derived from scanning those mock data.

annihilation channel. To know the annihilation channel further input would be required.

For the $\chi\chi \to \mu^+\mu^-$ case (left), the results depend on the mass of the dark matter particle. When the mock data contain a signal with $m_\chi = 15$ GeV (red circles and green squares), we can identify the properties of this signal relatively well. Our fits give masses and cross sections very close to the original ones. However, when the mock data contain a signal with $m_\chi = 30$ GeV (blue triangles and magenta diamonds), the signal becomes unidentifiable. Our fits give masses that span between 5 GeV and 50 GeV which is our entire tested mass range. Also, the cross section is very uncertain, spanning more than one order of magnitude around the original value. For the $m_\chi = 30$ GeV case, we used a smaller annihilation cross section to create the mock data. The presence of such dark matter doesn't deform the positron fraction spectrum significantly and our fitting procedure can adjust all the other astrophysical background parameters to fit the mock positron fraction very well. That is why for the more massive cases, the dark matter signal becomes unidentifiable. For the $m_\chi = 30$ GeV mock data, we picked the lower annihilation cross sections to $\mu^+\mu^-$, compared to the $m_\chi = 15$ GeV, as the relevant limits presented in Fig. 4, are stronger for the 30 GeV mass.

For the $\chi\chi \to \tau^+\tau^-$ case (right), it is much harder to identify the dark matter properties even when the mass is 15 GeV. When $m_\chi = 15$ GeV the cross sections that we decided to use to produce the mock data, deforms the positron fraction too much in the lowest energies where the error bars are the smallest. Our fits cannot adjust the astrophysical background parameters enough to fit this deformation. The end result is that for $\langle\sigma v\rangle = 1\times10^{-25}$ cm^3 s^{-1} (red circles), no fits survive within 2σ, while for $\langle\sigma v\rangle = 2\times10^{-26}$ cm^3 s^{-1} (green squares), only 3 fits are within 2σ. These 3 fits however fall around the original mass and the cross section that was used to create the mock data so our signal is identifiable within some uncertainty. When $m_\chi = 30$ GeV, the results are similar to the $\chi\chi \to \mu^+\mu^-$ case and the mass and annihilation cross section of the dark matter particle are completely unidentifiable for the same reasons.

IV. DISCUSSION AND CONCLUSIONS

In this paper we have used the most recent positron fraction measurement from AMS-02 to set upper limits on dark matter annihilation cross sections for masses of 5–120 GeV. Most of the electrons and positrons observed by AMS-02 do not originate from dark matter. Our astrophysical background modeling relies heavily on our previous work of Ref. [109]. The astrophysical backgrounds produced in that work are in agreement with a wide range of cosmic-ray measurements such as the positron fraction, the positron flux and the electron plus positron flux.

Our background models account for cosmic-ray primary electrons and uncertainties in their injection amplitude and spectrum, cosmic-ray secondary electrons and positrons and equivalent uncertainties in their injection amplitude and spectrum. They also include the contribution of Milky Way pulsars that come with a sequence of uncertainties. Those uncertainties are related to the stochastic

nature of their (neutron star) birth, distribution in space, initial spin-down power and the injected into the ISM cosmic-ray electron/positron fluxes. Pulsars also have a relatively uncertain time evolution as they spin down and also poorly determined efficiency in converting their rotational energy into cosmic-ray electrons and positrons. All these uncertainties are accounted for in our background simulations. Finally, we test a sequence of alternative modeling assumptions on how cosmic-ray electrons and positrons propagate through the ISM and the Heliosphere, before reaching the AMS-02 detector. In these background models we added a contribution from annihilating dark matter.

We study four different annihilation channels. These are $\chi\chi \to e^+e^-$, $\chi\chi \to \mu^+\mu^-$, $\chi\chi \to \tau^+\tau^-$ and $\chi\chi \to b\bar{b}$. We use a discretized grid of dark matter masses m_χ and test them over our large sample of astrophysical backgrounds. In our analysis the annihilation cross section, in units of $\langle\sigma v\rangle$ is treated as a free parameter. We derive upper limits on $\langle\sigma v\rangle$ as a function of m_χ for each annihilation channel which are summarized in Fig. 5.

We find that each valid astrophysical background that explains the *AMS-02* data well, gives different upper limits on $\langle\sigma v\rangle$. Therefore, we claim that the correct upper limits are not lines but bands spanning roughly one order of magnitude for each annihilation channel. We also find that the limits become stronger or weaker depending on the dark matter particle mass, and that this, in the $\chi\chi \to e^+e^-$ channel, has to do with low-energy spectral features in the positron fraction. To a weaker extend a similar trait exists for the $\chi\chi \to \mu^+\mu^-$ and $\chi\chi \to \tau^+\tau^-$ channels. Instead, the limits derived for the $\chi\chi \to b\bar{b}$ case are fairly insensitive to the existence of low-energy features in the positron fraction spectrum. We believe that a better understanding of the secondary production of cosmic rays in our Galaxy and solar modulation will help us to further refine these dark matter upper limits and reduce the widths of the presented bands. Modeling improvements as for instance those in [164,172] will be a step in the right direction.

Furthermore, we note that in the great majority of the astrophysical backgrounds that we use which are compatible with the $e^\pm$ observations by AMS-02, CALET and DAMPE, we still find preference for an additional cosmic-ray component. That component of 5–15 GeV $e^\pm$ is compatible with a dark matter contribution. However, its statistical significance varies between backgrounds and in a small fraction among them the preference for dark matter becomes negligible. We do not think that "excess" to be robust due to astrophysical background modeling uncertainties. The AMS-02 error bars at the low end of the energy range that we use are of the order of 0.5%. That is why the presence of a dark matter flux that contributes at the few percent level to the positron fraction can have a significant impact while fitting to the data. With future cosmic-ray measurements as for instance AMS-02 or an even more sensitive future cosmic-ray detector [182], we will be able to reduce these uncertainties and further scrutinize the positron fraction at that energy range.

Additionally, we created mock data of the AMS-02 positron fraction to check whether we could detect a dark matter signal contributing to its spectrum and also identify that signals' particle physics properties. We find that if dark matter contributes approximately 2–3% of the positron fraction in at least a few low-energy bins, we would be able to recognize the presence of some additional term in the AMS-02 data. However, determining the annihilation channel of such a signal is very challenging. If in such an analysis we allow for knowledge of the underlying annihilation channel, then for certain masses it is possible to accurately identify the dark matter properties of our injected mock dark matter signal.

We find that for dark matter annihilating to $\mu^+\mu^-$, for masses $m_\chi \sim 15$ GeV and cross sections $\langle\sigma v\rangle \sim 10^{-26}$ cm^3 s^{-1}, we can identify the properties of mock signals within some statistical uncertainty. For larger dark matter masses, the properties of the mock signals to $\mu^+\mu^-$ become more challenging. For dark matter annihilating to $\tau^+\tau^-$, we find that for masses $m_\chi \sim 15$ GeV and cross sections of the order of $\sim 1 \times 10^{-25}$ cm^3 s^{-1}, it is difficult to fit to the mock data with our models. For larger masses, the situation is similar to the $\mu^+\mu^-$ case where the properties of the dark matter signal are very uncertain.

We have made publicly available our dark matter fluxes in their prefitted format for the entire set. These files can be found at https://zenodo.org/record/7178634. Our astrophysical background models of Ref. [109], are instead available at https://zenodo.org/record/5659004.

ACKNOWLEDGMENTS

We thank Dan Hooper for useful discussions and Tim Linden and Isabelle John for comments on the manuscript. We also acknowledge the use of GALPROP [150,151] and the PYTHON [183] modules, NumPy [184], SciPy [174], PANDAS [185,186], MATPLOTLIB [187], JUPYTER [188], and IMINUIT [175,176]. I. C. acknowledges support from the Michigan Space Grant Consortium, NASA Grant No. 80NSSC20M0124. I. C. acknowledges that this material is based upon work supported by the U.S. Department of Energy, Office of Science, Office of High Energy Physics, under Award No. DE-SC0022352.

APPENDIX A: SUMMARY OF THE FULL PARAMETER SPACE

In this appendix we present briefly the parameter space that we test with our astrophysical background models and provide the ranges that the nuisance parameters are allowed to take. This parameter space can be seen in Table I. The last eight parameters in this Table are free fitting parameters that are optimized while fitting our simulations while the rest of the parameters are fixed and each astrophysical

TABLE I. List of parameters in our models. The last eight parameters are free fitting parameters and are optimized in our minimization procedure. The rest of the parameters are fixed and are different for each astrophysical pulsar background that we use. For more details on these parameters, refer to Secs. II and III of Ref. [109]. The last eight parameters are ranges of values while the rest are discreet sets separated by commas.

Parameter	Range
Galactic halo height, z_L [kpc]	3.0, 5.5, 5.7, 6.0
Energy-loss rate, b [10^{-6} GeV^{-1} kyrs^{-1}]	2.97, 5.05, 8.02
Diffusion coefficient, D_0 [pc^2 kyr^{-1}]	33.7, 51.3, 92.1, 140.2
Diffusion spectral index, δ	0.33, 0.40, 0.43, 0.50
Pulsar braking index, κ	2.5, 2.75, 3.0, 3.25, 3.5
Pulsar characteristic spin-down timescale, τ_0 [kyr]	$0.6, \ldots, 33$
Pulsar initial spin-down power cutoff, x_{cutoff}	$38.0, \ldots, 39.3$
Pulsar initial spin-down power mean, μ_y	$0.1, \ldots, 0.6$
Pulsar initial spin-down power standard deviation, σ_y	$0.25, \ldots, 0.75$
Pulsar cosmic-ray $e^{\pm}$ injection spectral index, n	Uniform distribution $\in$ [1.4,1.9], [1.6,1.7], [1.3,1.5]
Pulsar mean efficiency $\bar{\eta}$ and $\zeta = 10^{\sqrt{\text{variance}}}$ of $\bar{\eta}$ in $e^{\pm}$ pairs	$(4 \times 10^{-3}, 1.47)$, $(1 \times 10^{-3}, 2.85)$, $(1 \times 10^{-2}, 1.29)$
Prim. e^- flux normalization, a from reference value (see Ref. [109])	0.6–1.2
Sec. $e^{\pm}$ flux normalization, b from reference value (see Ref. [109])	0.8–2.0
Pulsar $e^{\pm}$ flux normalization, c	Such that $\bar{\eta} \cdot c \leq 0.5$
Prim. e^- flux spectral index modifier, d_1 from reference value (Ref. [109])	−0.2–0.5
Sec. $e^{\pm}$ flux spectral index modifier, d_2 from reference value (Ref. [109])	−0.1–0.1
Solar modulation parameter, ϕ_0 [GV]	0.1–0.6
Solar modulation parameter, ϕ_1 [GV]	0.0–2.0
Dark matter $e^{\pm}$ flux normalization, f	0.0–∞

background model has a unique set of pulsar parameters. Not all combinations of astrophysical parameters are allowed based on various observations from pulsars or cosmic rays. For more details on the properties of the constructed astrophysical backgrounds and the parameters describing them, please refer to Secs. II and III of Ref. [109]. The last eight parameters are presented as ranges while the rest are discrete sets separated by commas.

APPENDIX B: DIFFERENT STATISTICAL PROCEDURE

In this appendix, we explore a different statistical method for setting upper limits to the dark matter annihilation cross section. In our main analysis, we used a test statistic that tests the presence of a dark matter signal against the null hypothesis of purely conventional astrophysical sources to set our upper limits, i.e., $\langle \sigma v \rangle = 0$, which lies at the boundary of our parameter space. For this, we made use of Wilks' [178] and Chernoff's [179] theorems. We will now discuss a slightly different approach that as we show gives similar upper limits. Our combined upper-limit bands are roughly the same between the two methods.

Alternatively to the main text, we can use the test statistic,

$$LR(\langle \sigma v \rangle) = -2 \log \frac{\mathcal{L}(\langle \sigma v \rangle, \vec{\theta}_{\max})}{\mathcal{L}(\langle \hat{\sigma v} \rangle, \hat{\vec{\theta}})}, \tag{B1}$$

which is equal to a χ^2 difference. With $\vec{\theta}$ we denote all the nuisance parameters of the astrophysical background, while with hats we denote the parameters that maximize the likelihood function. According to Wilks' theorem, this test statistic follows a χ^2 distribution with one degree of freedom since now we do not have a hypothesis that lies on the boundary of our parameter space.

Following the standard convention in literature, we can deduce a 95% upper limit on the parameter $\langle \sigma v \rangle$, by the following procedure. For a fixed annihilation channel and dark matter mass, we find the parameters $\langle \hat{\sigma v} \rangle$ and $\hat{\vec{\theta}}$ that maximize the likelihood function, and then increase $\langle \sigma v \rangle$ until the test statistic LR reaches the value 3.84. Within that procedure, $\vec{\theta}_{\max}$ are the values of the astrophysical nuisance parameters that maximize the likelihood for a given value of $\langle \sigma v \rangle$. This method of profile likelihood is also called the MINOS method in high-energy physics.

The upper limits with this method appear to be similar to the ones created with the method of our main analysis for almost every background. For that reason we include Fig. 8, where we also show the upper limits with this method for the backgrounds of Fig. 3. From this figure, we can see that the upper limits set by this slightly different statistical methodology that doesn't rely on Chernoff's theorem are similar to the ones of our main analysis. That is true for every background that we use to construct our upper limit bands. Therefore we claim that the final combined bands of Fig. 5 are robust to both astrophysical background uncertainties and also to the statistical treatment of the positron fraction measurement.

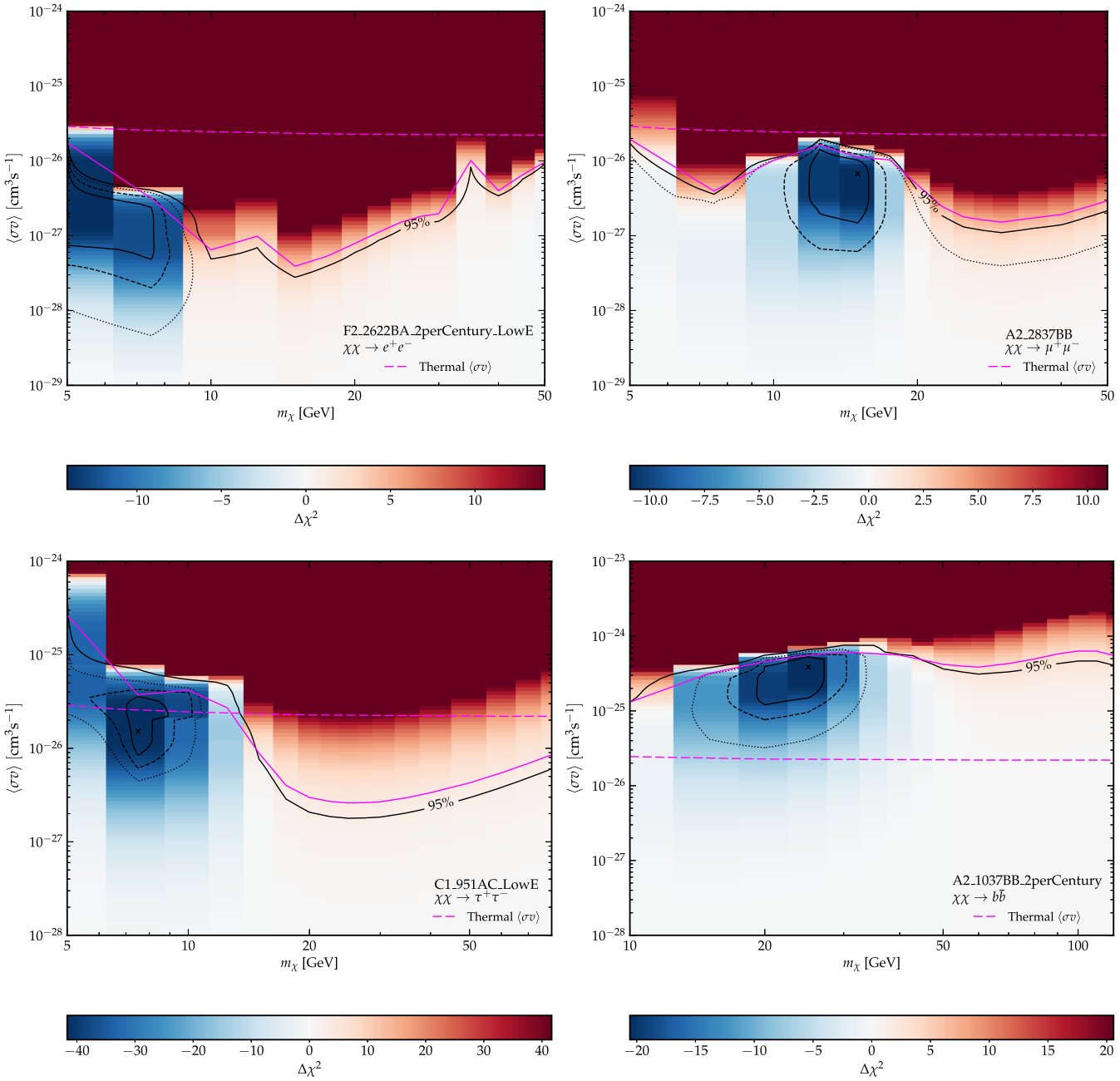

FIG. 8. Similar to Fig. 3, where for the same one background per channel, we show in solid magenta lines the upper limits derived by our second statistical method.

[1] Joshua D. Simon and Marla Geha, The kinematics of the ultra-faint Milky Way satellites: Solving the missing satellite problem, Astrophys. J. **670**, 313 (2007).
[2] Joshua D. Simon, The faintest dwarf galaxies, Annu. Rev. Astron. Astrophys. **57**, 375 (2019).
[3] Beth Willman, Julianne J. Dalcanton, David Martinez-Delgado, Andrew A. West, Michael R. Blanton, David W. Hogg, J. C. Barentine, Howard J. Brewington, Michael Harvanek, S. J. Kleinman, Jurek Krzesinski, Dan Long, Jr. Neilsen, Eric H., Atsuko Nitta, and Stephanie A. Snedden, A new Milky Way dwarf galaxy in ursa major, Astrophys. J. Lett. **626**, L85 (2005).
[4] Beth Willman, Michael R. Blanton, Andrew A. West, Julianne J. Dalcanton, David W. Hogg, Donald P.

Schneider, Nicholas Wherry, Brian Yanny, and Jon Brinkmann, A new Milky Way companion: Unusual globular cluster or extreme dwarf satellite? Astron. J. **129**, 2692 (2005).
[5] Paolo Salucci, The distribution of dark matter in galaxies, Astron. Astrophys. Rev. **27**, 2 (2019).
[6] Riccardo Catena and Piero Ullio, A novel determination of the local dark matter density, J. Cosmol. Astropart. Phys. 08 (2010) 004.
[7] Fabio Iocco, Miguel Pato, Gianfranco Bertone, and Philippe Jetzer, Dark matter distribution in the Milky Way: Microlensing and dynamical constraints, J. Cosmol. Astropart. Phys. 11 (2011) 029.
[8] Miguel Pato, Fabio Iocco, and Gianfranco Bertone, Dynamical constraints on the dark matter distribution in the Milky Way, J. Cosmol. Astropart. Phys. 12 (2015) 001.
[9] Jo Bovy and Scott Tremaine, On the local dark matter density, Astrophys. J. **756**, 89 (2012).
[10] Steven W. Allen, August E. Evrard, and Adam B. Mantz, Cosmological parameters from observations of galaxy clusters, Annu. Rev. Astron. Astrophys. **49**, 409 (2011).
[11] Vincent Desjacques, Donghui Jeong, and Fabian Schmidt, Large-scale galaxy bias, Phys. Rep. **733**, 1 (2018).
[12] Douglas Clowe, Marusa Bradac, Anthony H. Gonzalez, Maxim Markevitch, Scott W. Randall, Christine Jones, and Dennis Zaritsky, A direct empirical proof of the existence of dark matter, Astrophys. J. Lett. **648**, L109 (2006).
[13] J. R. Brownstein and J. W. Moffat, The bullet cluster 1E0657-558 evidence shows modified gravity in the absence of dark matter, Mon. Not. R. Astron. Soc. **382**, 29 (2007).
[14] Éric Aubourg *et al.*, Cosmological implications of baryon acoustic oscillation measurements, Phys. Rev. D **92**, 123516 (2015).
[15] John E. Carlstrom, Gilbert P. Holder, and Erik D. Reese, Cosmology with the Sunyaev-Zel'dovich Effect, Annu. Rev. Astron. Astrophys. **40**, 643 (2002).
[16] Ryan J. Cooke, Max Pettini, and Charles C. Steidel, One percent determination of the primordial deuterium abundance, Astrophys. J. **855**, 102 (2018).
[17] N. Aghanim *et al.* (Planck Collaboration), Planck 2018 results. VI. Cosmological parameters, Astron. Astrophys. **641**, A6 (2020); Erratum, Astron. Astrophys. **652**, C4 (2021).
[18] Nils Schöneberg, Julien Lesgourgues, and Deanna C. Hooper, The BAO + BBN take on the Hubble tension, J. Cosmol. Astropart. Phys. 10 (2019) 029.
[19] Fabio Iocco, Gianpiero Mangano, Gennaro Miele, Ofelia Pisanti, and Pasquale D. Serpico, Primordial nucleosynthesis: From precision cosmology to fundamental physics, Phys. Rep. **472**, 1 (2009).
[20] Maxim Pospelov and Josef Pradler, Big bang nucleosynthesis as a probe of new physics, Annu. Rev. Nucl. Part. Sci. **60**, 539 (2010).
[21] Richard H. Cyburt, Brian D. Fields, Keith A. Olive, and Tsung-Han Yeh, Big bang nucleosynthesis: 2015, Rev. Mod. Phys. **88**, 015004 (2016).
[22] A. Cuoco, F. Iocco, G. Mangano, G. Miele, Ofelia Pisanti, and P. D. Serpico, Present status of primordial nucleosynthesis after WMAP: Results from a new BBN code, Int. J. Mod. Phys. A **19**, 4431 (2004).
[23] Simon D. M. White and Carlos S. Frenk, Galaxy formation through hierarchical clustering, Astrophys. J. **379**, 52 (1991).
[24] Erik J. Tollerud, James S. Bullock, Louis E. Strigari, and Beth Willman, Hundreds of Milky Way satellites? Luminosity bias in the satellite luminosity function, Astrophys. J. **688**, 277 (2008).
[25] Nicolas G. Busca *et al.*, Baryon acoustic oscillations in the Ly-α forest of BOSS quasars, Astron. Astrophys. **552**, A96 (2013).
[26] Andrey V. Kravtsov and Stefano Borgani, Formation of galaxy clusters, Annu. Rev. Astron. Astrophys. **50**, 353 (2012).
[27] A. Mantz, S. W. Allen, D. Rapetti, and H. Ebeling, The observed growth of massive galaxy clusters—I. Statistical methods and cosmological constraints, Mon. Not. R. Astron. Soc. **406**, 1759 (2010).
[28] Lars Hernquist, Neal Katz, David H. Weinberg, and Jordi Miralda-Escudé, The Lyman-alpha forest in the cold dark matter model, Astrophys. J. Lett. **457**, L51 (1996).
[29] Antonella Garzilli, Andrii Magalich, Oleg Ruchayskiy, and Alexey Boyarsky, How to constrain warm dark matter with the Lyman-α forest, Mon. Not. R. Astron. Soc. **502**, 2356 (2021).
[30] I. Yu. Kobzarev, L. B. Okun, and I. Ya. Pomeranchuk, On the possibility of experimental observation of mirror particles, Sov. J. Nucl. Phys. **3**, 837 (1966).
[31] Bernard J. Carr and S. W. Hawking, Black holes in the early Universe, Mon. Not. R. Astron. Soc. **168**, 399 (1974).
[32] P. Meszaros, The behaviour of point masses in an expanding cosmological substratum, Astron. Astrophys. **37**, 225 (1974).
[33] B. J. Carr, The primordial black hole mass spectrum, Astrophys. J. **201**, 1 (1975).
[34] Steven Weinberg, A New Light Boson?, Phys. Rev. Lett. **40**, 223 (1978).
[35] Frank Wilczek, Problem of Strong P and T Invariance in the Presence of Instantons, Phys. Rev. Lett. **40**, 279 (1978).
[36] John Preskill, Mark B. Wise, and Frank Wilczek, Cosmology of the invisible axion, Phys. Lett. **120B**, 127 (1983).
[37] Michael Dine and Willy Fischler, The not so harmless axion, Phys. Lett. **120B**, 137 (1983).
[38] L. F. Abbott and P. Sikivie, A cosmological bound on the invisible axion, Phys. Lett. **120B**, 133 (1983).
[39] Z. G. Berezhiani, A. D. Dolgov, and R. N. Mohapatra, Asymmetric inflationary reheating and the nature of mirror universe, Phys. Lett. B **375**, 26 (1996).
[40] Peter Svrcek and Edward Witten, Axions in string theory, J. High Energy Phys. 06 (2006) 051.
[41] Matthew J. Strassler, Possible effects of a hidden valley on supersymmetric phenomenology, arXiv:hep-ph/0607160.
[42] Dan Hooper and Kathryn M. Zurek, A natural supersymmetric model with MeV dark matter, Phys. Rev. D **77**, 087302 (2008).
[43] Nima Arkani-Hamed and Neal Weiner, LHC signals for a superunified theory of dark matter, J. High Energy Phys. 12 (2008) 104.

[44] Lawrence J. Hall, Karsten Jedamzik, John March-Russell, and Stephen M. West, Freeze-in production of FIMP dark matter, J. High Energy Phys. 03 (2010) 080.
[45] Jonathan L. Feng, Dark matter candidates from particle physics and methods of detection, Annu. Rev. Astron. Astrophys. **48**, 495 (2010).
[46] Peter W. Graham, David E. Kaplan, and Surjeet Rajendran, Cosmological Relaxation of the Electroweak Scale, Phys. Rev. Lett. **115**, 221801 (2015).
[47] Gianfranco Bertone and Dan Hooper, History of dark matter, Rev. Mod. Phys. **90**, 045002 (2018).
[48] Yonit Hochberg, Eric Kuflik, Tomer Volansky, and Jay G. Wacker, Mechanism for Thermal Relic Dark Matter of Strongly Interacting Massive Particles, Phys. Rev. Lett. **113**, 171301 (2014).
[49] Yonit Hochberg, Eric Kuflik, Hitoshi Murayama, Tomer Volansky, and Jay G. Wacker, Model for Thermal Relic Dark Matter of Strongly Interacting Massive Particles, Phys. Rev. Lett. **115**, 021301 (2015).
[50] M. Drewes *et al.*, A white paper on keV sterile neutrino dark matter, J. Cosmol. Astropart. Phys. 01 (2017) 025.
[51] Yonatan Kahn, Gordan Krnjaic, Siddharth Mishra-Sharma, and Tim M. P. Tait, Light weakly coupled axial forces: Models, constraints, and projections, J. High Energy Phys. 05 (2017) 002.
[52] Simeon Bird, Ilias Cholis, Julian B. Muñoz, Yacine Ali-Haïmoud, Marc Kamionkowski, Ely D. Kovetz, Alvise Raccanelli, and Adam G. Riess, Did LIGO Detect Dark Matter?, Phys. Rev. Lett. **116**, 201301 (2016).
[53] Bernard Carr, Florian Kuhnel, and Marit Sandstad, Primordial black holes as dark matter, Phys. Rev. D **94**, 083504 (2016).
[54] Marco Battaglieri *et al.*, US Cosmic Visions: New Ideas in Dark Matter 2017: Community Report, arXiv:1707.04591.
[55] Gary Steigman, Basudeb Dasgupta, and John F. Beacom, Precise relic WIMP abundance and its impact on searches for dark matter annihilation, Phys. Rev. D **86**, 023506 (2012).
[56] Leszek Roszkowski, Enrico Maria Sessolo, and Sebastian Trojanowski, WIMP dark matter candidates and searches—current status and future prospects, Rep. Prog. Phys. **81**, 066201 (2018).
[57] Kim Griest and Marc Kamionkowski, Unitarity Limits on the Mass and Radius of Dark Matter Particles, Phys. Rev. Lett. **64**, 615 (1990).
[58] John F. Gunion, Howard E. Haber, Gordon L. Kane, and Sally Dawson, *The Higgs Hunter's Guide* (Brookhaven National Laboratory, Upton, New York, 2000), Vol. 80.
[59] Lisa Goodenough and Dan Hooper, Possible evidence for dark matter annihilation in the inner Milky Way from the fermi gamma ray space telescope, arXiv:0910.2998.
[60] Vincenzo Vitale and Aldo Morselli (Fermi-LAT Collaboration), Indirect search for dark matter from the center of the Milky Way with the fermi-large area telescope, arXiv:0912.3828.
[61] Dan Hooper and Lisa Goodenough, Dark matter annihilation in the galactic center as seen by the fermi gamma ray space telescope, Phys. Lett. B **697**, 412 (2011).
[62] Dan Hooper and Tim Linden, On the origin of the gamma rays from the galactic center, Phys. Rev. D **84**, 123005 (2011).
[63] Chris Gordon and Oscar Macias, Dark matter and pulsar model constraints from galactic center Fermi-LAT gamma ray observations, Phys. Rev. D **88**, 083521 (2013); Erratum, Phys. Rev. D **89**, 049901 (2014).
[64] Tansu Daylan, Douglas P. Finkbeiner, Dan Hooper, Tim Linden, Stephen K. N. Portillo, Nicholas L. Rodd, and Tracy R. Slatyer, The characterization of the gamma-ray signal from the central Milky Way: A case for annihilating dark matter, Phys. Dark Universe **12**, 1 (2016).
[65] Francesca Calore, Ilias Cholis, and Christoph Weniger, Background model systematics for the fermi GeV excess, J. Cosmol. Astropart. Phys. 03 (2015) 038.
[66] Francesca Calore, Ilias Cholis, Christopher McCabe, and Christoph Weniger, A tale of tails: Dark matter interpretations of the fermi GeV excess in light of background model systematics, Phys. Rev. D **91**, 063003 (2015).
[67] Kevork N. Abazajian, Nicolas Canac, Shunsaku Horiuchi, and Manoj Kaplinghat, Astrophysical and Dark matter interpretations of extended gamma-ray emission from the galactic center, Phys. Rev. D **90**, 023526 (2014).
[68] M. Ajello *et al.* (Fermi-LAT Collaboration), Fermi-LAT observations of high-energy γ-ray emission toward the galactic center, Astrophys. J. **819**, 44 (2016).
[69] Mattia Di Mauro, Characteristics of the galactic center excess measured with 11 years of *Fermi*-LAT data, Phys. Rev. D **103**, 063029 (2021).
[70] Ilias Cholis, Yi-Ming Zhong, Samuel D. McDermott, and Joseph P. Surdutovich, Return of the templates: Revisiting the galactic center excess with multimessenger observations, Phys. Rev. D **105**, 103023 (2022).
[71] Alessandro Cuoco, Michael Krämer, and Michael Korsmeier, Novel Dark Matter Constraints from Antiprotons in the Light of AMS-02, Phys. Rev. Lett. **118**, 191102 (2017).
[72] Ming-Yang Cui, Qiang Yuan, Yue-Lin Sming Tsai, and Yi-Zhong Fan, Possible Dark Matter Annihilation Signal in the AMS-02 Antiproton Data, Phys. Rev. Lett. **118**, 191101 (2017).
[73] Ilias Cholis, Tim Linden, and Dan Hooper, A robust excess in the cosmic-ray antiproton spectrum: Implications for annihilating dark matter, Phys. Rev. D **99**, 103026 (2019).
[74] Alessandro Cuoco, Jan Heisig, Lukas Klamt, Michael Korsmeier, and Michael Krämer, Scrutinizing the evidence for dark matter in cosmic-ray antiprotons, Phys. Rev. D **99**, 103014 (2019).
[75] M. Aguilar *et al.* (AMS Collaboration), The alpha magnetic spectrometer (AMS) on the international space station: Part II—Results from the first seven years, Phys. Rep. **894**, 1 (2021).
[76] M. Aguilar *et al.* (AMS Collaboration), Towards Understanding the Origin of Cosmic-Ray Positrons, Phys. Rev. Lett. **122**, 041102 (2019).
[77] Lars Bergstrom, Joakim Edsjo, and Piero Ullio, Cosmic anti-protons as a probe for supersymmetric dark matter?, Astrophys. J. **526**, 215 (1999).
[78] Dan Hooper, James E. Taylor, and Joseph Silk, Can supersymmetry naturally explain the positron excess?, Phys. Rev. D **69**, 103509 (2004).

[79] Stefano Profumo and Piero Ullio, The Role of antimatter searches in the hunt for supersymmetric dark matter, J. Cosmol. Astropart. Phys. 07 (2004) 006.
[80] Torsten Bringmann and Pierre Salati, The galactic antiproton spectrum at high energies: Background expectation vs exotic contributions, Phys. Rev. D **75**, 083006 (2007).
[81] Miguel Pato, Dan Hooper, and Melanie Simet, Pinpointing cosmic ray propagation with The AMS-02 experiment, J. Cosmol. Astropart. Phys. 06 (2010) 022.
[82] Lars Bergstrom, Torsten Bringmann, Ilias Cholis, Dan Hooper, and Christoph Weniger, New Limits on Dark Matter Annihilation from AMS Cosmic Ray Positron Data, Phys. Rev. Lett. **111**, 171101 (2013).
[83] Alejandro Ibarra, Anna S. Lamperstorfer, and Joseph Silk, Dark matter annihilations and decays after the AMS-02 positron measurements, Phys. Rev. D **89**, 063539 (2014).
[84] Rebecca K. Leane, Tracy R. Slatyer, John F. Beacom, and Kenny C. Y. Ng, GeV-scale thermal WIMPs: Not even slightly ruled out, Phys. Rev. D **98**, 023016 (2018).
[85] Isabelle John and Tim Linden, Cosmic-ray positrons strongly constrain leptophilic dark matter, J. Cosmol. Astropart. Phys. 12 (2021) 007.
[86] O. Adriani *et al.*, An anomalous positron abundance in cosmic rays with energies 1.5–100 GeV, Nature (London) **458**, 607 (2009).
[87] O. Adriani *et al.* (PAMELA Collaboration), Cosmic-Ray Positron Energy Spectrum Measured by PAMELA, Phys. Rev. Lett. **111**, 081102 (2013).
[88] M. Ackermann *et al.*, Measurement of Separate Cosmic-Ray Electron and Positron Spectra with the Fermi Large Area Telescope, Phys. Rev. Lett. **108**, 011103 (2012).
[89] L. Accardo *et al.* (AMS Collaboration), High Statistics Measurement of the Positron Fraction in Primary Cosmic Rays of 0.5–500 GeV with the Alpha Magnetic Spectrometer on the International Space Station, Phys. Rev. Lett. **113**, 121101 (2014).
[90] M. Aguilar *et al.* (AMS Collaboration), Towards Understanding the Origin of Cosmic-Ray Electrons, Phys. Rev. Lett. **122**, 101101 (2019).
[91] A. K. Harding and R. Ramaty, The pulsar contribution to galactic cosmic ray positrons, Int. Cosmic Ray Conf. **2**, 92 (1987).
[92] A. M. Atoyan, F. A. Aharonian, and H. J. Völk, Electrons and positrons in the galactic cosmic rays, Phys. Rev. D **52**, 3265 (1995).
[93] F. A. Aharonian, A. M. Atoyan, and H. J. Voelk, High energy electrons and positrons in cosmic rays as an indicator of the existence of a nearby cosmic tevatron, Astron. Astrophys. **294**, L41 (1995).
[94] Dan Hooper, Pasquale Blasi, and Pasquale Dario Serpico, Pulsars as the sources of high energy cosmic ray positrons, J. Cosmol. Astropart. Phys. 01 (2009) 025.
[95] Hasan Yuksel, Matthew D. Kistler, and Todor Stanev, TeV Gamma Rays from Geminga and the Origin of the GeV Positron Excess, Phys. Rev. Lett. **103**, 051101 (2009).
[96] Stefano Profumo, Dissecting cosmic-ray electron-positron data with Occam's Razor: the role of known Pulsars, Central Eur. J. Phys. **10**, 1 (2011).
[97] Dmitry Malyshev, Ilias Cholis, and Joseph Gelfand, Pulsars versus dark matter interpretation of ATIC/PAMELA, Phys. Rev. D **80**, 063005 (2009).
[98] Norita Kawanaka, Kunihito Ioka, and Mihoko M. Nojiri, Cosmic-ray electron excess from pulsars is spiky or smooth?: Continuous and multiple electron/positron injections, Astrophys. J. **710**, 958 (2010).
[99] D. Grasso *et al.* (Fermi-LAT Collaboration), On possible interpretations of the high energy electron-positron spectrum measured by the Fermi Large Area Telescope, Astropart. Phys. **32**, 140 (2009).
[100] Jeremy S. Heyl, Ramandeep Gill, and Lars Hernquist, Cosmic rays from pulsars and magnetars, Mon. Not. R. Astron. Soc. **406**, L25 (2010).
[101] Tim Linden and Stefano Profumo, Probing the pulsar origin of the anomalous positron fraction with AMS-02 and atmospheric Cherenkov telescopes, Astrophys. J. **772**, 18 (2013).
[102] Ilias Cholis and Dan Hooper, Dark matter and pulsar origins of the rising cosmic ray positron fraction in light of new data from AMS, Phys. Rev. D **88**, 023013 (2013).
[103] Q. Yuan, X.-J. Bi, G.-M. Chen, Y.-Q. Guo, S.-J. Lin, and X. Zhang, Implications of the AMS-02 positron fraction in cosmic rays, Astropart. Phys. **60**, 1 (2015).
[104] Peng-Fei Yin, Zhao-Huan Yu, Qiang Yuan, and Xiao-Jun Bi, Pulsar interpretation for the AMS-02 result, Phys. Rev. D **88**, 023001 (2013).
[105] Ilias Cholis, Tanvi Karwal, and Marc Kamionkowski, Studying the Milky Way pulsar population with cosmic-ray leptons, Phys. Rev. D **98**, 063008 (2018).
[106] Carmelo Evoli, Elena Amato, Pasquale Blasi, and Roberto Aloisio, Galactic factories of cosmic-ray electrons and positrons, Phys. Rev. D **103**, 083010 (2021).
[107] Silvia Manconi, Mattia Di Mauro, and Fiorenza Donato, Detection of a γ-ray halo around Geminga with the *Fermi*-LAT and implications for the positron flux, Proc. Sci., ICRC2019 (**2021**) 580.
[108] Luca Orusa, Silvia Manconi, Fiorenza Donato, and Mattia Di Mauro, Constraining positron emission from pulsar populations with AMS-02 data, J. Cosmol. Astropart. Phys. 12 (2021) 014.
[109] Ilias Cholis and Iason Krommydas, Utilizing cosmic-ray positron and electron observations to probe the averaged properties of Milky Way pulsars, Phys. Rev. D **105**, 023015 (2022).
[110] Pasquale Blasi, The Origin of the Positron Excess in Cosmic Rays, Phys. Rev. Lett. **103**, 051104 (2009).
[111] Philipp Mertsch and Subir Sarkar, Testing Astrophysical Models for the PAMELA Positron Excess with Cosmic Ray Nuclei, Phys. Rev. Lett. **103**, 081104 (2009).
[112] Markus Ahlers, Philipp Mertsch, and Subir Sarkar, On cosmic ray acceleration in supernova remnants and the FERMI/PAMELA data, Phys. Rev. D **80**, 123017 (2009).
[113] Pasquale Blasi and Pasquale D. Serpico, High-Energy Antiprotons from Old Supernova Remnants, Phys. Rev. Lett. **103**, 081103 (2009).
[114] Norita Kawanaka, Kunihito Ioka, Yutaka Ohira, and Kazumi Kashiyama, TeV electron spectrum for probing cosmic-ray escape from a supernova remnant, Astrophys. J. **729**, 93 (2011).

[115] Yutaka Fujita, Kazunori Kohri, Ryo Yamazaki, and Kunihito Ioka, Is the PAMELA anomaly caused by the supernova explosions near the Earth?, Phys. Rev. D **80**, 063003 (2009).
[116] M. Di Mauro, F. Donato, N. Fornengo, R. Lineros, and A. Vittino, Interpretation of AMS-02 electrons and positrons data, J. Cosmol. Astropart. Phys. 04 (2014) 006.
[117] Kazunori Kohri, Kunihito Ioka, Yutaka Fujita, and Ryo Yamazaki, Can we explain AMS-02 antiproton and positron excesses simultaneously by nearby supernovae without pulsars or dark matter?, Prog. Theor. Exp. Phys. **2016**, 021E01 (2016).
[118] Philipp Mertsch, Stochastic cosmic ray sources and the TeV break in the all-electron spectrum, J. Cosmol. Astropart. Phys. 11 (2018) 045.
[119] Ilias Cholis and Dan Hooper, Constraining the origin of the rising cosmic ray positron fraction with the boron-to-carbon ratio, Phys. Rev. D **89**, 043013 (2014).
[120] Philipp Mertsch and Subir Sarkar, AMS-02 data confront acceleration of cosmic ray secondaries in nearby sources, Phys. Rev. D **90**, 061301 (2014).
[121] Ilias Cholis, Dan Hooper, and Tim Linden, Possible evidence for the stochastic acceleration of secondary antiprotons by supernova remnants, Phys. Rev. D **95**, 123007 (2017).
[122] Nicola Tomassetti and Alberto Oliva, Production and acceleration of antinuclei in supernova shockwaves, Astrophys. J. **844**, L26 (2017).
[123] Daniele Gaggero, Luca Maccione, Giuseppe Di Bernardo, Carmelo Evoli, and Dario Grasso, Three-Dimensional Model of Cosmic-Ray Lepton Propagation Reproduces Data from the Alpha Magnetic Spectrometer on the International Space Station, Phys. Rev. Lett. **111**, 021102 (2013).
[124] R. Cowsik, B. Burch, and T. Madziwa-Nussinov, The origin of the spectral intensities of cosmic-ray positrons, Astrophys. J. **786**, 124 (2014).
[125] Daniele Gaggero, Luca Maccione, Dario Grasso, Giuseppe Di Bernardo, and Carmelo Evoli, PAMELA and AMS-02 e^+ and e^- spectra are reproduced by three-dimensional cosmic-ray modeling, Phys. Rev. D **89**, 083007 (2014).
[126] Lars Bergstrom, Torsten Bringmann, and Joakim Edsjo, New positron spectral features from supersymmetric dark matter—a way to explain the PAMELA data?, Phys. Rev. D **78**, 103520 (2008).
[127] Marco Cirelli and Alessandro Strumia, Minimal Dark Matter predictions and the PAMELA positron excess, Proc. Sci., IDM2008 (**2008**) 089 [arXiv:0808.3867].
[128] Ilias Cholis, Lisa Goodenough, Dan Hooper, Melanie Simet, and Neal Weiner, High energy positrons from annihilating dark matter, Phys. Rev. D **80**, 123511 (2009).
[129] Marco Cirelli, Mario Kadastik, Martti Raidal, and Alessandro Strumia, Model-independent implications of the e+-, anti-proton cosmic ray spectra on properties of dark matter, Nucl. Phys. **B813**, 1 (2009); **B873**, 530(A) (2013).
[130] Ann E. Nelson and Christopher Spitzer, Slightly non-minimal dark matter in PAMELA and ATIC, J. High Energy Phys. 10 (2010) 066.
[131] Nima Arkani-Hamed, Douglas P. Finkbeiner, Tracy R. Slatyer, and Neal Weiner, A theory of dark matter, Phys. Rev. D **79**, 015014 (2009).
[132] Ilias Cholis, Douglas P. Finkbeiner, Lisa Goodenough, and Neal Weiner, The PAMELA positron excess from annihilations into a light boson, J. Cosmol. Astropart. Phys. 12 (2009) 007.
[133] Ilias Cholis, Gregory Dobler, Douglas P. Finkbeiner, Lisa Goodenough, and Neal Weiner, The case for a 700+ GeV WIMP: Cosmic ray spectra from ATIC and PAMELA, Phys. Rev. D **80**, 123518 (2009).
[134] Roni Harnik and Graham D. Kribs, An effective theory of dirac dark matter, Phys. Rev. D **79**, 095007 (2009).
[135] Patrick J. Fox and Erich Poppitz, Leptophilic dark matter, Phys. Rev. D **79**, 083528 (2009).
[136] Maxim Pospelov and Adam Ritz, Astrophysical signatures of secluded dark matter, Phys. Lett. B **671**, 391 (2009).
[137] John David March-Russell and Stephen Mathew West, WIMPonium and boost factors for indirect dark matter detection, Phys. Lett. B **676**, 133 (2009).
[138] Spencer Chang and Lisa Goodenough, Charge asymmetric cosmic ray signals from dark matter decay, Phys. Rev. D **84**, 023524 (2011).
[139] Keith R. Dienes, Jason Kumar, and Brooks Thomas, Dynamical Dark Matter and the positron excess in light of AMS results, Phys. Rev. D **88**, 103509 (2013).
[140] Douglas P. Finkbeiner and Neal Weiner, Exciting dark matter and the INTEGRAL/SPI 511 keV signal, Phys. Rev. D **76**, 083519 (2007).
[141] Joachim Kopp, Constraints on dark matter annihilation from AMS-02 results, Phys. Rev. D **88**, 076013 (2013).
[142] P. S. Bhupal Dev, Dilip Kumar Ghosh, Nobuchika Okada, and Ipsita Saha, Neutrino mass and dark matter in light of recent AMS-02 results, Phys. Rev. D **89**, 095001 (2014).
[143] Michael Klasen, Martin Pohl, and Günter Sigl, Indirect and direct search for dark matter, Prog. Part. Nucl. Phys. **85**, 1 (2015).
[144] Qiang Yuan and Lei Feng, Dark matter particle explorer observations of high-energy cosmic ray electrons plus positrons and their physical implications, Sci. China Phys. Mech. Astron. **61**, 101002 (2018).
[145] Xudong Sun and Ben-Zhong Dai, Dark matter annihilation into leptons through gravity portals, J. High Energy Phys. 04 (2021) 108.
[146] Carmelo Evoli, Tim Linden, and Giovanni Morlino, Self-generated cosmic-ray confinement in TeV halos: Implications for TeV γ-ray emission and the positron excess, Phys. Rev. D **98**, 063017 (2018).
[147] Ilias Cholis, Tanvi Karwal, and Marc Kamionkowski, Features in the spectrum of cosmic-ray positrons from pulsars, Phys. Rev. D **97**, 123011 (2018).
[148] O. Adriani *et al.*, Extended Measurement of the Cosmic-Ray Electron and Positron Spectrum from 11 GeV to 4.8 TeV with the Calorimetric Electron Telescope on the International Space Station, Phys. Rev. Lett. **120**, 261102 (2018).
[149] G. Ambrosi *et al.* (DAMPE Collaboration), Direct detection of a break in the teraelectronvolt cosmic-ray spectrum of electrons and positrons, Nature (London) **552**, 63 (2017).

[150] A. W. Strong and I. V. Moskalenko, Propagation of cosmic-ray nucleons in the galaxy, Astrophys. J. **509**, 212 (1998).
[151] https://galprop.stanford.edu/.
[152] Igor V. Moskalenko, Troy A. Porter, and Andrew W. Strong, Attenuation of vhe gamma rays by the Milky Way interstellar radiation field, Astrophys. J. Lett. **640**, L155 (2006).
[153] Troy A. Porter and A. W. Strong, A new estimate of the galactic interstellar radiation field between 0.1 microns and 1000 microns, in *Proceedings of the 29th International Cosmic Ray Conference* (2005), arXiv:astro-ph/0507119.
[154] Troy A. Porter, Gudlaugur Johannesson, and Igor V. Moskalenko, High-energy gamma rays from the Milky Way: Three-dimensional spatial models for the cosmic-ray and radiation field densities in the interstellar medium, Astrophys. J. **846**, 67 (2017).
[155] G. Ambrosi *et al.* (DAMPE Collaboration), Direct detection of a break in the teraelectronvolt cosmic-ray spectrum of electrons and positrons, Nature (London) **552**, 63 (2017).
[156] P. Salucci, F. Nesti, G. Gentile, and C. F. Martins, The dark matter density at the Sun's location, Astron. Astrophys. **523**, A83 (2010).
[157] Julio F. Navarro, Carlos S. Frenk, and Simon D. M. White, The Structure of cold dark matter halos, Astrophys. J. **462**, 563 (1996).
[158] Marco Cirelli, Gennaro Corcella, Andi Hektor, Gert Hutsi, Mario Kadastik, Paolo Panci, Martti Raidal, Filippo Sala, and Alessandro Strumia, PPPC 4 DM ID: A poor particle physicist cookbook for dark matter indirect detection, J. Cosmol. Astropart. Phys. 03 (2011) 051.
[159] R. Trotta, G. Johannesson, I. V. Moskalenko, T. A. Porter, R. Ruiz de Austri, and A. W. Strong, Constraints on cosmic-ray propagation models from a global Bayesian analysis, Astrophys. J. **729**, 106 (2011).
[160] Ilias Cholis, Dan Hooper, and Tim Linden, A predictive analytic model for the solar modulation of cosmic rays, Phys. Rev. D **93**, 043016 (2016).
[161] Ilias Cholis, Dan Hooper, and Tim Linden, Constraining the charge-sign and rigidity-dependence of solar modulation, J. Cosmol. Astropart. Phys. 10 (2022) 051.
[162] Ilias Cholis and Ian McKinnon, Constraining the charge-, time- and rigidity-dependence of cosmic-ray solar modulation with AMS-02 observations during solar cycle 24, Phys. Rev. D **106**, 063021 (2022).
[163] M. J. Boschini, S. Della Torre, M. Gervasi, D. Grandi, G. Jóhannesson, G. La Vacca, N. Masi, I. V. Moskalenko, S. Pensotti, T. A. Porter, L. Quadrani, P. G. Rancoita, D. Rozza, and M. Tacconi, Deciphering the local interstellar spectra of primary cosmic-ray species with HELMOD, Astrophys. J. **858**, 61 (2018).
[164] M. J. Boschini, S. Della Torre, M. Gervasi, G. La Vacca, and P. G. Rancoita, The transport of galactic cosmic rays in Heliosphere: The helmod model compared with other commonly employed solar modulation models, Adv. Space Res. **70**, 2636 (2022).
[165] Rolf Kappl, SOLARPROP: Charge-sign dependent solar modulation for everyone, Comput. Phys. Commun. **207**, 386 (2016).
[166] M. S. Potgieter, The global modulation of cosmic rays during a quiet Heliosphere: A mod eling perspective, Adv. Space Res. **60**, 848 (2017).
[167] R. D. Strauss, M. S. Potgieter, I. Büsching, and A. Kopp, Modelling heliospheric current sheet drift in stochastic cosmic ray transport models, Astrophys. Space Sci. **339**, 223 (2012).
[168] Gang Qin and Zhenning Shen, Modulation of galactic cosmic rays in the inner Heliosphere, comparing with pamela measurements, Astrophys. J. **846**, 56 (2017).
[169] Matteo Jerome Boschini, Stefano Della Torre, Massimo Gerv asi, Giuseppe La Vacca, and Pier Giorgio Rancoita, The helmod model in the works for inner and outer Heliosphere: From AMS to voyager probes observations, Adv. Space Res. **64**, 2459 (2019).
[170] R. A. Caballero-Lopez, N. E. Engelbrecht, and J. D. Richardson, Correlation of long-term cosmic-ray modulation with solar activity par ameters, Astrophys. J. **883**, 73 (2019).
[171] D. Bisschoff, M. S. Potgieter, and O. P. M. Aslam, new very local interstellar spectra for electrons, positrons, protons, and light cosmic ray nuclei, Astrophys. J. **878**, 59 (2019).
[172] Jung-Tsung Li, John F. Beacom, and Annika H. G. Peter, Galactic cosmic-ray propagation in the inner Heliosphere: Improve d force-field model, Astrophys. J. **937**, 27 (2022).
[173] Luca Orusa, Mattia Di Mauro, Fiorenza Donato, and Michael Korsmeier, New determination of the production cross section for secondary positrons and electrons in the Galaxy, Phys. Rev. D **105**, 123021 (2022).
[174] P. Virtanen *et al.*, SciPy 1.0: Fundamental algorithms for scientific computing in python, Nat. Methods **17**, 261 (2020).
[175] Hans Dembinski, Piti Ongmongkolkul *et al.*, scikit-hep/iminuit, 10.5281/zenodo.3949207 (2020).
[176] F. James and M. Roos, MINUIT: A system for function minimization and analysis of the parameter errors and correlations, Comput. Phys. Commun. **10**, 343 (1975).
[177] Ilias Cholis and Iason Krommydas, Possible counterpart signal of the Fermi bubbles at the cosmic-ray positrons, arXiv:2208.07880.
[178] S. S. Wilks, The large-sample distribution of the likelihood ratio for testing composite hypotheses, Ann. Math. Stat. **9**, 60 (1938).
[179] Herman Chernoff, On the distribution of the likelihood ratio, Ann. Math. Stat. **25**, 573 (1954).
[180] Jan Conrad, Statistical issues in astrophysical searches for particle dark matter, Astropart. Phys. **62**, 165 (2015).
[181] A. Albert *et al.* (Fermi-LAT and DES Collaborations), Searching for dark matter annihilation in recently discovered Milky Way satellites with Fermi-LAT, Astrophys. J. **834**, 110 (2017).
[182] S. Schael *et al.*, AMS-100: The next generation magnetic spectrometer in space—An international science platform for physics and astrophysics at Lagrange point 2, Nucl. Instrum. Methods Phys. Res., Sect. A **944**, 162561 (2019).
[183] Guido Van Rossum and Fred L. Drake, *PYTHON 3 Reference Manual* (CreateSpace, Scotts Valley, CA, 2009).
[184] Charles R. Harris *et al.*, Array programming with NumPy, Nature (London) **585**, 357 (2020).

[185] J. Reback *et al.*, pandas-dev/pandas: PANDAS1.4.2, 10.5281/zenodo.3509134 (2020).

[186] Wes McKinney, Data structures for statistical computing in python, in *Proceedings of the 9th Python in Science Conference*, edited by Stéfan van der Walt and Jarrod Millman (2010), pp. 56–61.

[187] J. D. Hunter, MATPLOTLIB: A 2d graphics environment, Comput. Sci. Eng. **9**, 90 (2007).

[188] Thomas Kluyver *et al.*, *JUPYTER notebooks—a publishing format for reproducible computational workflows* (IOS Press, Southampton, United Kingdom, 2016), pp. 87–90.